Instituto Tecnológico y de Estudios Superiores de Monterrey

Campus Monterrey
School of Engineering and Sciences

**TECNOLÓGICO
DE MONTERREY** ®

Implementation of a transient approach for the mass and energy balance
in an electric arc furnace.
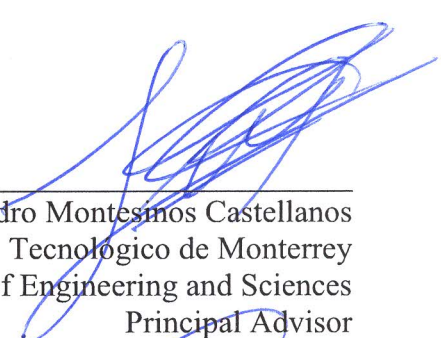
A thesis presented by
Alejandra Camacho Pasos

Submitted to the
School of Engineering and Sciences
in partial fulfillment of the requirements for the degree of
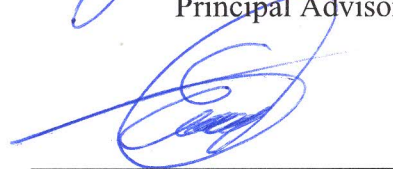
Master of Science
In
Energy Engineering

Monterrey Nuevo León, November 28th, 2018

Instituto Tecnológico y de Estudios Superiores de Monterrey

Campus Monterrey
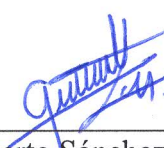
School of Engineering and Sciences

The committee members, hereby, certify that have read the thesis presented by Alejandra Camacho Pasos and that it is fully adequate in scope and quality as a partial requirement for the degree of Master of Science in Energy Engineering.

Dr. Alejandro Montesinos Castellanos
Tecnológico de Monterrey
School of Engineering and Sciences
Principal Advisor

Dr. Eder Trejo Treviño
Ternium México, S.A. de C.V.
Co-advisor

M Sc. Gilberto Sánchez Cisneros
Ternium México, S.A. de C.V.
Committee Member

Dr. Rubén Morales Menéndez
Dean of Graduate Studies
School of Engineering and Sciences

Monterrey Nuevo León, November 28th, 2018

Declaration of Authorship

I, Alejandra Camacho Pasos, declare that this thesis titled, Implementation of a transient approach for the mass and energy balance in an electric arc furnace, and the work presented in it are my own. I confirm that:

- This work was done wholly or mainly while in candidature for a research degree at this University.
- Where any part of this thesis has previously been submitted for a degree or any other qualification at this University or any other institution, this has been clearly stated.
- Where I have consulted the published work of others, this is always clearly attributed.
- Where I have quoted from the work of others, the source is always given. With the exception of such quotations, this thesis is entirely my own work.
- I have acknowledged all main sources of help.
- Where the thesis is based on work done by myself jointly with others, I have made clear exactly what was done by others and what I have contributed myself.

Alejandra Camacho Pasos
Monterrey Nuevo León, December 28,th 2018

Dedication

I dedicate this thesis to my family for all your unconditional support, love and encouragement. All of you are my motivation to reach all my objectives in my life, without you, this wouldn't have been possible.

Acknowledgements

First, I want to thank to the almighty God for establishing me to finish my master's degree and giving me the wisdom and the strength.

I would like to express my whole gratitude to my family for encouraging me in this important step of my life and for always being my inspiration.

I am highly indebted to SENER and CONACYT for their help on tuition and living support which made possible this research. For the company Ternium for the collaborative efforts and the information providing.

I want to thank to my advisors, Dr. Alejandro Montesinos and Dr. Eder Trejo for their guidance through the development of this work.

Thanks to Dr. Osvaldo Micheloud for giving me this great opportunity, in which I had invaluable experiences and I knew extraordinary people.

And last, my thanks and appreciation for my partners at the consortium and people who have willingly helped me with their abilities.

Abstract

On this work, an implementation of a transient approach for the mass and energy balance in an electric arc furnace is presented. Real operation conditions were included, such as the dynamic material and energy additions and continuous inlets and outlets. Also, several inherent phenomena were characterized, such as the melting rate of scrap, the chemical reaction mechanisms and the residence time of bubbles in the slag. With all these elements, the estimation of the distribution of mass and energy flows at any time of the "heat" process was performed. The main contributions of this work are to provide a prediction of mass and energy distribution at any time of the EAF process, and to be a guideline for a dynamic optimization model which can be useful to improve the efficiency of the furnace by operation protocol modifications, therefore, the net cost per ton of liquid steel can be reduced.

List of figures

List of tables

Contents

Chapter I

Introduction

On the present work, a comprehensive transient approach for the mass and energy balance in an electric arc furnace (EAF) is presented. Real operation conditions were modeled, such as additions of material and power, dynamic streams of mass and energy, and several inherent phenomena. Thus, this model is able to simulate the whole process of a batch of liquid steel (often called "heat"). This work was structured as follows:

- **Chapter I. Introduction**. Explanation of the context of this research: background of the steel industry, its importance, its social-economic influence worldwide, types of steel making processes and main steps. Also, the statement of the problem, the scopes, the objectives and the justification are explained in this section.

- **Chapter II. State of the art.** The scientific basis to establish this model is presented, covering the existing mass and energy balance (MEB) models and their main modules.

- **Chapter III. Methodology.** The available resources, the suppositions, the considerations and the employed methods for building of the model.

- **Chapter IV. Results and discussion.** Since the most relevant result was the mass and energy balance structure as such, a detailed description of the model and important modules was made:
    1. The material-energy additions,
    2. The melting rate,
    3. The kinetics in liquid metal and slag zone,
    4. The bubbles residence,
    5. The minimization of Gibbs free energy in gases,

Also, in this chapter some simulations were performed, obtaining the estimations for infiltrations and off gases, the mass accumulation and the mass and energy balances. Besides, in order to test the reliability of the kinetic model, a sensitive analysis was made.

- **Chapter V.** Conclusions, contributions and future work.

1.1 Background

It is a fact that the energy is one of the main inputs to guarantee sustainability, competitiveness and development for the industry. For this reason, over the five last decades, efficient usage and environmental care have gathered more concerning, thus, the efforts in research and development for this area have increased.

According to International Energy Agency, in 2015 the total industry energy consumption accounted for 37% (392,889.3 PJ) of the global delivered energy, from this percentage, the iron and steel sector represented 20.1 % (IEA, 2017). A similar scenario is presented in the Mexican context, then, in 2016 the industry final consumption represented 31.7% (1,680.79 PJ) and from this percentage, 14.4% corresponded to iron and steel sector (SENER, 2017), being the largest industrial consumer in Mexico. As the last statistical data showed, the steel industry is a great consumer of energy and the furnaces are fundamental equipment for the production, the improvement of their efficiencies is one of the main challenges on this field.

1.1.1   Steel industry

The steel has a preponderant influence and presence in our life almost everywhere, a huge number of daily things that cover needs and conveniences for mankind are made of this material, such as pipelines, transmission towers, building structures, machine parts, etc. Due to its mechanical, multi-functionality, adaptability, recycling and plenty on earth, it is the most suitable metallic material to employ. Besides, the steel production costs are lower than other metals production costs. For instance, just 25 % of the energy needed for aluminum extraction is enough to extract iron (SAIL co., 2017).

Moreover, the iron and steel industry has been an important pillar of some nation economies, in Mexico this industry plays a preponderant role due to the high production (19.9 million of ton) and

the exportation of steel (5.1 million of ton) (Canacero, 2018); indeed, this country is placed in the 14st place of steel production worldwide (Association, 2017).

On the other hand, as this industry always has been an intensive energy consumer, some energy solutions have been applied since 1960, such as more sophisticated equipment (electrodes, cooling panels, etc.), recovery of heat and energy management systems. As a result, the consumption has been reduced about 60% up to the present day (Association, 2016).

1.1.2 Types of melting process

The most expensive process in the steel mills is the primary steelmaking, that basically is the melting of raw material, in Figure 1.1 the main routes of production are displayed: The Blast Furnace-Basic Oxygen Furnace (BF-BOF) and the Electric Arc Furnace (EAF). Dotted lines indicate the parts of the routes that may be connected to each other.
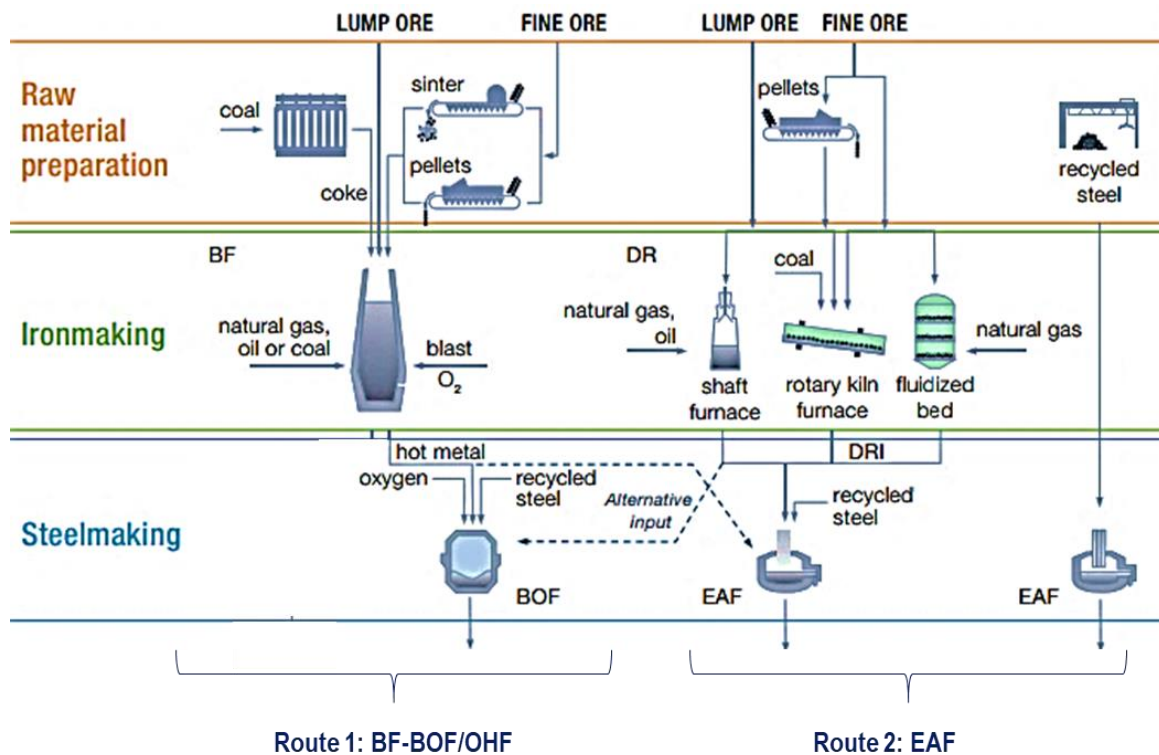
Figure 1.1 Main routes of steel production (Association, 2018).
BF: Blast furnace, **DR**: Direct reduction, **BOF**: Basic oxygen furnace and **EAF**: Electric arc furnace.

About 70 % (~ 1,119.65 million of ton per year) of the worldwide steel is produced by route 1 (Association, 2018), in which the main raw materials are the iron ores, and the coal. The ironmaking stage consists of smelting the iron ores while a hot blast of air enriched of oxygen are blown into the lower section as the ores are falling. These iron ores are reduced by combustion gases (CO, CO_2) to produce the intermediate product: pig iron. And last, either the pig iron or direct reduction iron DRI (dotted line) is fed into the Basic oxygen furnace where it is converted into steel.

By the route 2, about 30% (479.85 million of ton) of worldwide steel is produced, having as raw material the scrap (recycled steel), and as intermediate products the direct reduction iron (DRI) or the pig iron (dotted line). The preparation of scrap as raw material consists of a rigorous classification by chemical composition, level of impurity, size, shape and homogeneity. The main intermediate process of this route consists of reducing the oxygen content from the iron (oxide pellets or lump ores). The iron is fed into the top vessel of the shaft furnace (Figure 1.1), where it descents by gravity and preheated, then it is in contact with the reducing gas (hydrogen or carbon monoxide) at up to 1073 K obtaining heat/cold DRI or hot briquette iron (Midrex technologies, 2014). Subsequently, the smelting is carried out in the EAF. As this route uses a great percentage of scrap, it is also considered a recycling process and its production cost is lower in comparison with the other route.

1.1.3   Electric arc furnace and process description

The first installation of an electric arc furnace took place in Halcomb plant in United States in 1906 (Crucible industries, 2016), since then, this technology has not stop to evolved over the years, improving some of its components, for instance, larger transformers, cooled panels, direct current and ultrahigh power systems, and different arrangements for electrodes to obtain better efficiencies. From the point of view of type of current, the EAFs can be classified in alternate current (AC), which is the most used equipment, and direct current (DC). For the last one, there are different designs: one electrode and one anode in the bottom, and two electrodes with four anodes (Madias, 2013).

Basically, a modern EAF consists of cylinder container with a steel outer shell. The scrap is melted by graphite electrodes which emit an electric arc (plasma), refractory bricks cover the lowest part

of the EAF, whereas water cooled panels cover the roof; the full load (called "heat") is discharged through eccentric bottom tapping (EBT) into the teeming ladle. A feedback from the electrical system controls the position of the vertical displacement of the electrodes, depending on their voltage reading, they are raised or lowered.

The whole process in the EAF is carried out by batches called "heats" and the operation time is called "Tap-to-Tap time". Generally, this operation comprises of 6 main steps as shown in Figure 1.2 for a simple case.
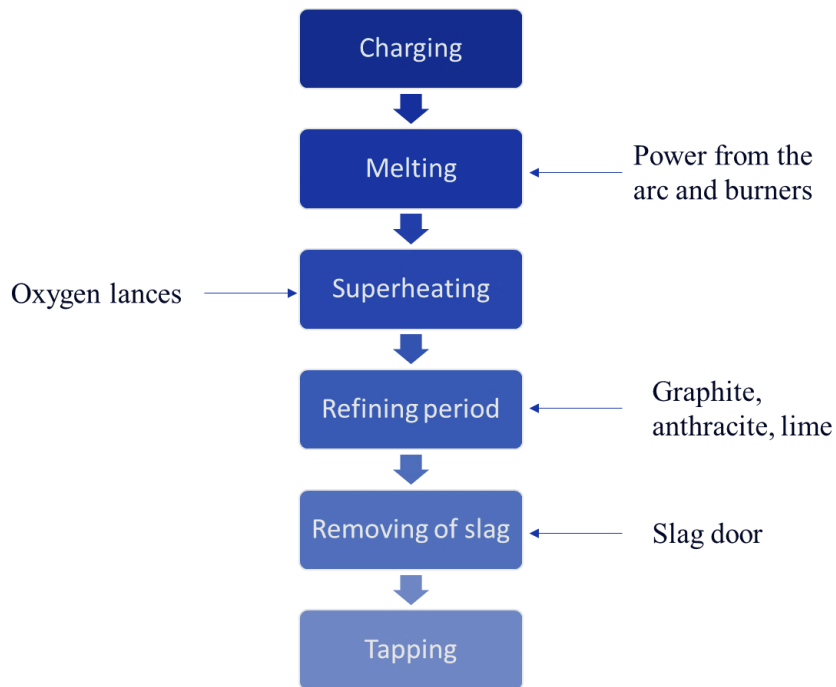
Figure 1.2 Main steps of a "heat" process .

1. **Charging.** After a thorough classification of the scrap, this is loaded in baskets and brought towards the furnace.

2. **Melting.** After the charging, the graphite electrodes bore down, and the power is supplied moderately to avoid arc hitting or damages on the equipment (Figure 1.3, A) , to compensate the weak radiation in the cold spots, the burners are employed to increase the energy in those areas. From this point the operation conditions change, ending with the melting down of the charge of scrap (Figure 1.3, B). then, either DRI or another charge of scrap is added to melt down again.

3. **Superheating.** In order to reach flat bath conditions at temperatures above 1863 K, the maximum power is supplied. Also, in this step, the oxygen is lanced with the purpose of obtaining extra energy due to the oxidation reactions (exothermic), simultaneously, this promotes the steel decarburization and production of carbon monoxide bubbles.
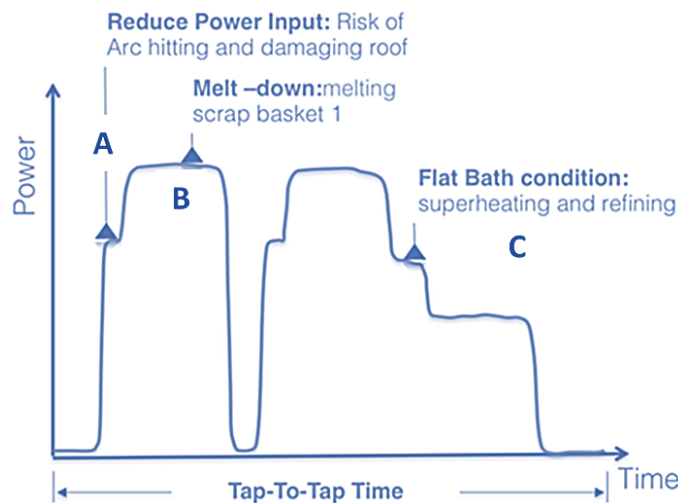
Figure 1.3 Power supply during the Tap-To-Tap time.

4. **Refining period**. Once the target tapping temperature (Figure 1.3 A) is reached the refining period starts with the addition of some reductant materials (graphite, anthracite or iron silicide) to recover more steel and valuable alloys.

5. **Removing of slag**. the slag is removed from the steel by spillage when the volume exceeds the split line (slag door level).

6. **Tapping**: this step must be performed very fast, there are two commons designs for tapping:

   • Eccentrically-Bottom Tapping (EBT): A tap hole is placed out of the center, on the bottom of the EAF, this permits a slag-free tapping into the teeming ladle. In this case a small amount of steel and slag, called "hot heel" is left between the "heats".

   • Spout: This configuration causes the slag carrying over the ladle where it is mixed with the steel. No hot heel is remained.

1.2 Problem statement and context

As statistical data shows (IEA, 2017; SENER, 2017), the iron and steel industry consumes a huge amount of energy per year, within the steel mills this is more noticeable on the melting furnaces. This work is focused on one of the most employed technologies for iron-steel melting: the electric arc furnace (EAF), in which even the minimum energy savings represents great achievements for production costs. As demonstrated in previous studies (Trejo, 2012), for a typical DC EAF most of the energy input is supplied by the electric energy (55.8%), the rest corresponds to the fuel energy and chemical energy, while the energy outputs correspond to the inherent energy of the liquid steel and slag (including "hot heel"), and the energy losses.

The energy losses are comprised mainly by the heat absorbed by the off gases and the heat of the cooling system, which account for about 40% of the energy input. The problem with them are their lack of direct harnessing and their impact on the efficiency reduction of the EAF. Nowadays there are some solutions to recover the residual heat from off gases, for instance, the preheating of metallic charge before its discharging to the EAF (TENOVA, 2017), also to decrease the energy transferred to the cooling system, good slag foaming practices are the best option.

Other problem is to maintain a balance on the level of oxidation. The lancing of oxygen contributes to obtain suitable flat bath temperatures, conversely, it produces more metallic oxides, in higher percentage iron oxide. To improve the yield, the recovery of *Fe* and alloys is carried out by reduction reactions which require carbon additions but decrease the bath temperature since they are endothermic.

To identify efficiency problems in the EAF, an overview of the energy distributions is needed, they could be estimated by the mass and energy balances (BME). Usually they have been performed in steady state, however, before the need of timely detection and real-time prediction, a transient approach is required. To attack the problem of high oxidation and slag treatments (related directly with efficiency problems), a composition profile and a mass change profile are required to be employed as a preliminary guideline for the improving of operation protocols.

As object of study, the analysis was performed for an DC EAF Fuchs® with capacity of 150 Ton/heat. This equipment is located at Ternium Guerrero plant, San Nicolas de los Garza, Nuevo

Leon, whose specifications are shown in Table 1.1. The main limitation of this equipment is the lack of instrumentation for the monitoring of concentration and temperature of the gases.

Table 1.1 Characteristics for DC EAF Fuchs ®.

Specifications	Value and units
Productivity	150 T/h
Type of EAF	Direct current
Oxygen lances	4
Burners	6 x 5 mW
Carbon system	4 insufflators continue load of carbon.
Lime system	2
Transformer capacity	3 x 52, 156 MVA
Electrodes diameter	28 in
Number of anodes (bottom)	3

1.3 General objective

To develop a comprehensive transient approach for the mass and energy balance in an electric arc furnace for the whole process of a "heat". The main purpose is to estimate mass and energy accumulations and distributions at any time of the heat, as a result, this overview will set the basis for a predictive model for the improving of energy efficiency practices and chemical treatment.

1.4 Specific objectives

- To estimate the inlets and outlets of mass and energy, including the unknowns: the infiltrations of air, the off gases and the spillage of slag.
- To estimate the melting rate of scrap considering the additions of energy and the proposed heat transfer mechanism, to compare with the other zones in the accumulation profiles.

- To propose chemical reaction mechanisms in the steel zone and in the slag zone and to estimate their reaction velocity. From this, to generate a composition (%wt.) profile to be compared with slag sampling.
- To establish some numerical factors to adjust the model for this furnace.
- To perform some simulations to test the coherence of the melting rate, the composition profiles, the temperatures and the mass and energy accumulations and distributions.
- To perform a sensitive analysis setting as output variable the composition of CO in the slag and as input variables the contents of carbon and iron oxide in DRI.

1.5 Scope

This work is focused on the implementation of a transient approach for the mass and energy balance in an electric arc furnace, by the employment of fundamental basis, it pretends to be robust and adaptable for any kind of EAF. This simulates the complete operation of a "heat" and considers the furnace as a control volume, where the mass and energy flows are dynamic, regarding this, the model covers:

- The input of the inlets of material and energy by addition profiles.
- The estimation of discrete inlets and outlets of mass and energy also including the unknown flows: the off gases, the infiltrations and the spillage of slag.
- The estimation of temperature profiles for gas zone and steel-slag zone.

The phenomena included within the model are:

- The melting rate of scrap, in which the energy supply from the arc and burners are involved, besides the heat transfer among the scrap, liquid steel and gases.
- The settlement of reaction mechanisms in the liquid metal and in the slag and chemical kinetics module.
- The residence time of the carbon monoxide bubbles as this is related to the kinetics.
- The chemical equilibria of gases.
- The energy addition or reduction of energy caused by the reactions.

To adapt the model for the specific equipment (EAF), it is adjusted by some numerical factors with a set of heats as it was made in previous works (Richard D. M. MacRosty, 2005), subsequently the coherence of the model is tested by the comparison between the simulations and operation data, and the change susceptibility by a sensitive analysis.

In addition, this model will be useful for the user (operators, process staff) since it is able to display the overview of mass and energy accumulations at any time of the heat, as well as the inlets and outlets distributions.

Conversely, the following is not considered:

- The oxidation of alloys (Cr, Mn, Ti, V), since they are in minimum quantities in the steel, from the energy point of view this is not relevant.
- The activities estimations for the components in the slag.
- The heat transfer model and the analysis of slag foaming in the arc coverage.

1.6 Justification

As explained previously, the estimation of mass and energy distribution is very important to detect opportunities to enhance efficiency and production of the EAF. Most of the estimation tools are performed in steady state, before the need of having a timely overview at any time, a transient approach is required.

The transient model could be useful for a better administration of flows of mass and energy, therefore preliminary solutions could be carried out. With a proper adjustment of this tool and the integration of a heat transfer model, it also could be employed as a guideline for an optimization model, which could help in making decisions for the improvement of operation protocols ("recipes").

According to some references about the effects of arc coverage and slag thickness in the panels (Trejo, 2012)(Treviño, 2012), to obtain cooling losses below 70 kWh/Ton, good practices of slag foaming must be applied to maintain at least of 80% of arc coverage and a slag layer of 3 cm. Since the cooling losses for this EAF (Fuchs ®) are around 80 kWh/Ton, with this model the necessary actions to decrease these losses can be carried out without affecting the other variables by the

observation of the dynamic behavior. With the reduction of 10 kWh/Ton per heat, considering an average of 150 TLS (Ton of liquid steel) and a plant factor of 90%, 30 MWh are saved per day, this is reflected on savings of 49,500 USD/month, taking as reference the mean price of 55 USD/MWh (from the electric energy generated in their self-supply plant Techgen).

Regarding the economic savings by the improvements of the yield of the production, assuming that 1 extra Ton of steel is recovered per "heat" and considering the current price of 463 USD/Ton of steel (Alacero, 2018), 283,356 USD/month are estimated as resulting savings.

Chapter II

State of art

2.1 Mass and energy balance model

Currently, there are several works that present total or partial estimations of the mass and energy flows in the EAF, most of them are considered for steady state. For instance, there are several analysis from the point view of exergy (Bisio, Rubatto and Martini, 2000; Çamdalı and Tunç, 2002; Çamdali and Tunç, 2003), in which the energy wastes in the cooling system were estimated by exergy factors and exergies associated to the streams, also, the efficiencies for the EAF were determined by the criteria of the second law of thermodynamics. In other works, the mass and energy conversion efficiencies were employed to simplify the complexity of the heat transfer mechanisms from the electric arc and the reactions of oxidation and combustion (Kirschen, Badr and Pfeifer, 2011). A different approach for the estimation of mass and energy balance employed a vector point of view in which the solving was performed by the minimization of the difference of inlets and outlets (Trejo, 2012), and the energy estimations were calculated by the concept of total enthalpy.

Previous references have different approaches and objectives, but they are performed in steady state, when the EAF is actually a kind of semi batch reactor, even though these models generate good estimations, they do not consider extensively the phenomena during the operation such as heat transfer mechanisms, chemical reactions, mass transfer, etc. Conversely, some comprehensive models were already developed (Bekker, Craig and Pistorius, 1999; Morales, Rodriguez-Hernández and Conejo, 2001; Richard D. M. MacRosty, 2005; Vito Logar and Skrjanc, 2012b, 2012c), they are a good guidelines, since they employed transient approaches and some inherent phenomena.

A mathematical simulator for an EAF fed with DRI was developed (Morales *et al.*, 1997), and it demonstrated to be good basis for the next models due to its robustness and the consideration of

the 3 main relevant reactions: oxidation, decarburization and reduction. To ease the estimation of kinetics, a division of the system and a proposed mechanism were employed.

Some simulations were presented for a closed loop control with the purpose of testing off gases variables such as concentrations and temperatures (Bekker, Craig and Pistorius, 1999). For the development of this work, some reasonable assumptions and simplifications were applied, for instance, the same temperatures for the liquid metal and the molten slag, the consideration of the most important metallurgical reactions (oxidation and reduction) and the instantaneous melting of DRI. The energy calculation was made by energy additions, total enthalpy and heat transfer. This model also considered the rate of change of liquid metal mass as a function of the melting rate of the scrap, the rate of oxidation of Fe, the rate of reduction of FeO and the DRI addition rate.

Following the last guideline, a more comprehensive model was developed (Richard D. M. MacRosty, 2005), in which the melting process, the chemical reaction mechanisms and the energy flows were characterized and the system was modeled by four equilibrium zones: gas zone, slag-metal interaction zone, molten steel zone and solid scrap zone, each one limited by the mass transfer principle. Due to the lack of knowledge of the complex nature of the mass interaction inside the EAF, the mass balance had an atomic approach and the chemical equilibrium was computed by minimizing Gibbs free energy with a first order solution. About the energy balance, the overall Equation 2-1 was used for each zone:

$$\frac{d}{dt}(E_z) = Q_z + \sum_{i=1}^{n} |\dot{m}_{iz} H_{iz}|_{in} - \sum_{i=1}^{n} |\dot{m}_{iz} H_{iz}|_{out} \qquad \text{2-1}$$

Where Q_z is the heat flow added to the zone z, $\dot{m}_{iz}$ is the mass flow per element and H_{iz} is the outlet/inlet corresponding enthalpy. The only inconvenient for the resulting simulator (Richard D. M. MacRosty, 2005) is the consumption of computational resources and time of running due to the complex optimization method.

From the two last models (Bekker, Craig and Pistorius, 1999; Richard D. M. MacRosty, 2005) another dynamic model was derived (Vito Logar and Skrjanc, 2012b, 2012c), where an analysis for mass transfer, heat and thermo-chemistry was performed, afterwards a dynamic simulator was built (Vito Logar and Skrjanc, 2012a). The study of the EAF was divided in 7 zones: solid scrap

zone, liquid scrap zone, solid slag zone, liquid slag zone, gas zone (lanced gases and oxidation/reduction gases), roof zone and wall zone. For each zone an energy balance is applied in detail considering conduction, convection and radiation. Despite the innovative and comprehensive approach, the conditions used are very simplified and idealized for the complex nature of EAF process and the chemical behavior.

A detailed analysis of energy losses was presented (Trejo *et al.*, 2012), it was based on the EAF efficiency and it analyzes thoroughly the electrical losses, electrical variables and chemical energy. The electrical losses were estimated by the randomness power theory, reaching up to 6% of the total energy input. The heat transfer considers energy transport equations of conduction, convection and radiation. Also, the losses by cooling system were strictly estimated by a radiation model, in which the view factors were obtained by a volume finite software. Regarding to the cooling system energy losses, the slag layer thickness adhered to the panels plays a very important role (Bisio, Rubatto and Martini, 2000). Then, different scenarios for the slag layer and arc coverage were already simulated (Trejo *et al.*, 2012), this permitted the calculation of thermal efficiencies, which were determined by Equation 2-2.

$$\eta_{EAF} = \frac{E_{stl}}{E_{arc} + E_{elo} + E_{chem}} \qquad \text{2-2}$$

Where, η_{EAF} is the efficiency of the EAF, E_{stl} is the inherent energy in the steel, E_{arc} is the energy from the arc, E_{elo} are the electrical losses and E_{chem} is the chemical energy. Also, this author proposed an overall balance that defines the unknown losses E_{OL} in the EAF, defined as Equation 2-3

$$\text{E}_{OL} = \sum Q_{in} - \sum Q_{out} + \sum W_{in} - \sum W_{out} + \sum \sum H_{Tin} - \sum \sum H_{T_{out}} \qquad \text{2-3}$$

Where $Q_{in} = 0$ because there is no thermal energy input; Q_{out} represents the thermal losses vector which includes: 1) Thermal losses in the cooling system, 2) electrical losses 3) thermal losses in the bottom of the furnace, 4) energy losses when the furnace is open, 5) energy losses by the slag

door hole and 6) cooling of the electrodes; $W_{out} = 0$ because there is no work output; H_{in} and H_{out} are the chemical inlets an outlets including the combustion.

Regarding to the incorporation of energies per specie, some models (Bekker, Craig and Pistorius, 2000; Richard D. M. MacRosty, 2005; Trejo, 2012) employed the concept of Total enthalpy, which includes the standard formation enthalpy $\widehat{H}_f^0$, the sensible heat (heat before reaching phase changes) and the latent heat (at change of phase). It should be noted that some species such as Fe, FeO, Fe_2O_3, have stages of transitions before reaching melting point limited by temperature ranges.

2.2 Melting rate

As mentioned before, the EAF process is a recycling process, since this produces a great amount of steel by scrap melting, this raw material covers about 30-60 percent of the production, thus, cost savings per ton of liquid steel (TLS) are higher. The estimation of melting rate of scrap gathers a great concerning for the dynamic simulations of EAF because it is necessary to know the liquid metal production and the proper time of some additions such as DRI and power. For a practical modelling a general analysis of the whole amount of scrap was taken and the resolution for individual pieces was discarded in the following models.

Melting rate modules were found in some mentioned models (Bekker, Craig and Pistorius, 1999; Richard D. M. MacRosty, 2005), and they were built on the basis of heat transfer mechanisms in which the operation complexity and the irregular scrap geometry were simplified by some reasonable suppositions and considerations.

The scrap melting was calculated as function of heat transfer for convection only from the liquid metal to the solid scrap (Bekker, Craig and Pistorius, 1999) which is proportional to the difference of temperatures and it was globally defined by Equation 2-4.

$$\dot{M}_{melt} = - \frac{M_{Fe} \cdot H_{therm_1} \cdot k_{area} \cdot m_{s_{iron}} \cdot (T_{ls} - T_{ss}) \cdot \left(\frac{T_{ss}}{T_{ls}}\right)}{\lambda_{Fe} + C_{p_{Fe(s)}}(T_{ls} - T_{ss})} \qquad 2\text{-}4$$

Where H_{therm1} is the heat transfer coefficient ($\frac{kW}{m^2 K}$), k_{area} is the contact area ($\frac{m^2}{kg}$) for the scrap in melting process, λ_{Fe} is the latent heat of fusion ($\frac{kJ}{mole}$) and $Cp_{Fe(s)}$ ($\frac{kJ}{kgK}$) the specific heat, which is multiplied by temperature difference. M_{Fe} is the average molar mass of iron, $m_{S_{iron}}$ is the mass of solid iron, T_{ls} is the liquid metal temperature, T_{ss} is the solid scrap temperature.

On the other hand, a more complete structure with the 3 heat transfer mechanisms was represented (Richard D. M. MacRosty, 2005). The melting rate of the scrap $\dot{M}_{melt}$ was determined by dividing the available energy for the scrap to be melted by the energy required to melt the scrap at a given temperature (Equation 2-5).

$$\dot{M}_{melt} = \frac{Q_{ss}\left(\frac{T_{ss}}{T_{melt}}\right)}{\left[\Delta H_{f,Fe} + \int_{T_s}^{T_{melt}} C_{p,Fe(s)}dT\right] \cdot \kappa_{dm}} \qquad \text{2-5}$$

T_{melt} is the melting point temperature, $\frac{T_{ss}}{T_{melt}}$ represents the fraction of energy that contributes to the melting of the scrap, $\Delta H_{f,Fe}$ is the heat of fusion of Fe, κ_{dm} is an adjusting parameter, T_s is the temperature of the scrap trough melting process and it is obtained by Equation 2-6.

$$\frac{d}{dx}(T_s) = \frac{Q_{ss}\left(1 - \frac{T_{ss}}{T_{melt}}\right) - \dot{M}_{scrap}\int_{T_0}^{T_s} C_{p,Fe(s)}dT}{\left[m_{ss} \cdot C_{p,Fe(s)}\right]\kappa_{dT}} \qquad \text{2-6}$$

Where $\dot{M}_{scrap}$ is the rate of addition of scrap and m_{ss} is the mass of solid steel. Q_{ss} is the total energy transferred to the scrap (Equation 2-7).

$$Q_{ss} = Q_{power-ss} + Q_{mm-ss} + Q_{gas-ss} - Q_{volatile} - \dot{q}_3^{rad} \qquad \text{2-7}$$

$Q_{power-ss}$ is the electrical energy transferred from the arc to solid scrap, Q_{mm-ss} heat from molten metal to solid scrap, Q_{gas-ss} heat from gas zone to solid scrap, $Q_{volatile}$ is the energy content in the solid scrap required to vaporize volatile components and q_3^{rad} is the energy lost by radiation from the scrap.

A more classified approach for melting furnaces was presented and it was applied to an aluminum melting furnace (Wu and Lacroix, 1995), where two-dimensions were considered and the complexity of the problem was dealt with an enthalpy-porosity method. In this alternative, the domain was taken as a pseudo porous medium with the purpose to simulate the pieces of scrap and the voids among them, and the process stages were divided as shown in Figure 2.1.
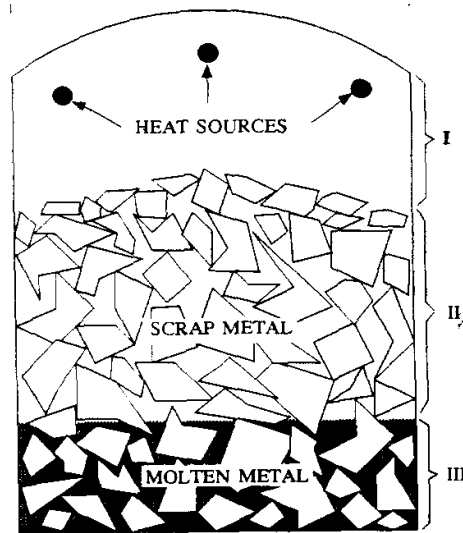
Figure 2.1 Division of the melting stages in a melting furnace for aluminum (Wu and Lacroix, 1995).

I.   **Heating stage**: the burners heat the scrap at the top of the furnace. The heat is transferred by the flame, by the gases among the voids and by the conduction piece-piece.

II.   **Melting stage**: as the melting occurs, the liquid metal moves down the bottom of the furnace. At the same time the pieces of scrap are heated by the flame and liquid steel in the low boundary. Here the interphases gas-solid and solid-liquid exist simultaneously.

III. **Final stage:** once the whole scrap is submerged, just the interphase solid-liquid exists.

The heat transfer mechanisms identified for each stage are: in I forced convection (flame) and radiation by arc gases; in II, conduction in pieces and convection/radiation in voids; in III conduction and convection by the metal liquid bath. The governing energy equation employed were Equation 2-8, assuming axisymmetric flow respect to central vertical axis.

$$\rho C_p \frac{\partial T}{\partial t} = \frac{\partial}{\partial x}\left(K\frac{\partial T}{\partial x}\right) + \frac{\partial}{\partial y}\left(K\frac{\partial T}{\partial y}\right) - \rho\lambda_{Fe}\frac{\partial f_l}{\partial t} + \dot{q}'' \qquad \text{2-8}$$

x, y are the coordinates, K is the thermal conductivity of the pieces. The heat flux was estimated by Equation 2-9, considering that the flame penetrates deeply through the voids and it decreases in axial form. $\rho\lambda_{Fe}\frac{\partial f_l}{\partial t}$ is the enthalpy formulation for the interphase solid-liquid.

$$\dot{q}'' = \dot{q}_0 e^{-\beta x} \qquad \text{2-9}$$

Where q_0 is the value of heat flux at the top of the scrap and β is the flame blocking factor. For the region III the heat flux for convection is represented by Equation 2-10 only.

$$\dot{q}'' = h_l A_{eff}(T_b - T) \qquad \text{2-10}$$

Where h_l is the convection coefficient, A_{eff} is the effective area and T_b is the solid block temperature.

2.3 Reaction mechanisms

Chemical reactions play a crucial role during the heat since they are one of the main sources of energy and they participate in the refining of the steel and in the slag foaming. Due to the complexity of the reactions in the melting process, there are few proposed mechanisms. Some of them were found in some literature (Zhang and Fruehan, 1995; Morales *et al.*, 1997; Morales, Rodriguez-Hernández and Conejo, 2001; Steel University, 2015) and they were focused on the liquid steel- slag interaction.

The main objectives of the oxygen lancing are to supply extra energy into the flat bath and to eliminate some carbon content from the steel (decarburization). The oxygen lances impinge directly into the liquid steel, causing the oxidation (Equation 2-11) and the decarburization (Equation 2-12) reactions. The lead products are iron oxide *FeO* and carbon monoxide *CO* (exhibited as bubbles), which are transferred to the slag zone.

$$Fe_l + \frac{1}{2}O_2 \rightarrow FeO$$

2-11

$$C + \frac{1}{2}O_2 \rightarrow CO$$

2-12

In order to counteract the percentage of *FeO* and to produce more slag foaming, graphite and carbon derivates are added into the slag. As *CO* molecules are produced and raised into the slag,
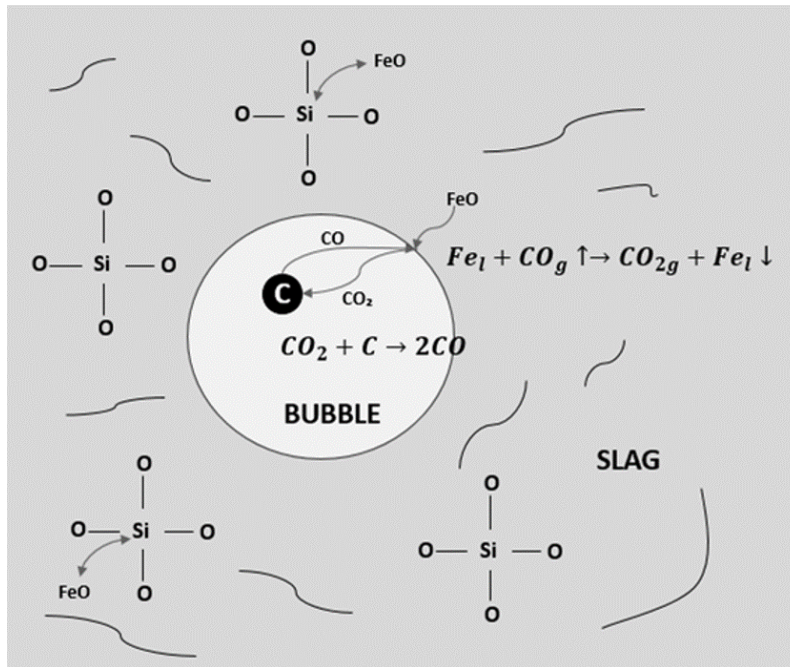
Figure 2.2 Reaction mechanism for slag (Morales et al., 1997).

they are nucleated (forming a gas halo) due to the supersaturation of carbon (Morales *et al.*, 1997) as shown in Figure 2.2. The activity of *FeO* is conditioned by silica content, since it has a larger

particle size, thus, it causes the limitation of available reaction surface for the iron oxide in the CO-CO_2 bubble.

When FeO reaches the free surface on a bubble, the reaction of reduction with CO takes place (Equation 2-13) forming carbon dioxide CO_2 and recovering Fe.

$$FeO_l + CO_g \rightarrow CO_{2(g)} \uparrow + Fe_l \downarrow \qquad\qquad 2\text{-}13$$

CO_2 reacts with the carbon particles (trapped in the bubble), where the CO is regenerated by reaction of Boudouard (Equation 2-14).

$$CO_{2(g)} + C \rightarrow 2\,CO_g \qquad\qquad 2\text{-}14$$

Regarding to the insufflated addition of graphite, some demonstrations (Morales *et al.*, 1995) indicated that in acid slags (higher content of silica) small graphite particle sizes ($100 - 150\mu m$) show higher rates of reduction and the kinetics is controlled by gas-liquid interface; whereas in the basic slags, larger sizes ($300 - 500\,\mu m$) show higher reduction rates and the reaction is controlled by mass transfer.

In addition, previous experiments (Tanaka *et al.*, 2016) also indicated other important reduction reaction (Equation 2-15), which produces more stable CO bubbles than those ones produced by the reaction of Equation 2-13. Stable bubbles help to form true foaming, that is enough stable and lasts several minutes after stopping gas generation.

$$2\text{-}15$$
$$FeO + C \rightarrow Fe_l \downarrow + CO \downarrow$$

It is obvious that carbon monoxide is the critical component to obtain a proper foamability, but also some properties influence to achieve it: surface tension, viscosity and density. These properties can be upgraded by changing some chemical properties.

2.4 Minimization of Gibbs free energy: Gases

Due to the lack of knowledge of reaction mechanisms in gases and their competition, a good alternative is the minimization of the Gibbs free energy of the mixture (White, Johnson and Dantzig, 1958), this procedure enables the determination of the concentrations at equilibrium points. For the case of the EAF, $P = 1\ atm$ and the temperatures are high, at this conditions, the total Gibbs free energy (G) and the activities of components are defined by Equation 2-16 and Equation 2-17 respectively.

$$\frac{G}{RT} = \sum_{i=1}^{c} n_i \left(\frac{G_i^\circ}{RT} + Ln\frac{n_i}{n} \right) \tag{2-16}$$

$$\frac{\overline{f_i}}{f_i^0} = \frac{n_i}{n} \tag{2-17}$$

Where G° is the Gibbs free energy of formation, $\frac{\overline{f_i}}{f_i^0}$ is the activities of the components, n_i is the mole quantity of the components and n is the total quantity of mole in the reacting mixture. The objective is to find the species compositions corresponding to $\frac{G}{RT}$; the problem lies in finding acceptable combinations for n_i which are constrained for the conservation of the atomic species, then the relationship of the Equation 2-18 must satisfy them.

$$\sum_{i=1}^{c} a_{ji} n_i = b_j \qquad \text{for}\ \ 1 \leq j \leq M \tag{2-18}$$

Where a_{ji} are the number of atoms-grams of the atomic element (j) within a mole of molecules (i); b_j total number of atoms-grams from the elements (j) in the reacting mixture; and M is the number of present elements.

Some modifications were applied by the employment of iterations and an approximated solution of the minimum (Richard Balzhiser, 1972), at last iteration the problem is simplified using Lagrange multipliers λ'_j (they remain constant until the end) as shown in Equation 2-19

.

$$0 = \frac{G_i^0}{RT} \, \mathrm{Ln} \frac{n_i}{n} - \sum_{j=1}^{M} \lambda'_i a_{ji}$$

2-19

Subsequently, the estimation of molar contents is obtained by the solving for n_i, Equation 2-20:

$$n_i = n \exp\left(\sum_{j=1}^{M} \lambda'_j a_{ji} - \frac{G_i^0}{RT}\right)$$

2-20

2.5 Slag foaming

During the heat, the slag is produced by the oxide contents from the inlet materials and the injection of oxygen, a certain amount of this is desirable to improve the furnace efficiency, since it helps:

- To maintain the electric arc submerged, this decreases the energy losses by radiation into the furnace walls.
- To protect the refractories from the arc.
- To cover the cooling panels with the slag layer.

To take advantages of the mentioned benefits, a stable foam production is necessary when the graphite particles are injected, and bubbles are produced. These bubbles stay within the slag for a while, the longer they keep, the more stable foaming is.

The slag foaming phenomena has been studied for a long time (Mills and Keene, 1987; Ito and Fruehan, 1989; Zhang and Fruehan, 1995; Sekino, Nagasaka and Fruehan, 2000; Li and Fruehan, 2003; Matsuura and ard J. Fruehan, 2009) and it has been already proven that the density ρ, viscosity μ, and surface tension σ of the slag have an important influence on the ability of the slag to form a stable foam. Most of the models calculate these properties with empirical basis.

From reported data of densities and surface tensions in *CaO-MgO-SiO₂* systems (Mills and Keene, 1987), a regression analysis was performed (Morales *et al.*, 1997) to obtain the expressions for the corresponding properties at steelmaking temperature, Equation 2-21 and 2-22:

$$\rho = 2460 + 18(\text{FeO Wt. \%}) \qquad\qquad 2\text{-}21$$

$$\sigma = 0.75424 - 0.5694 \left(\text{wt. \%} \frac{SiO_2}{100} \right) - 0.13713 \left(\text{wt. \%} \frac{FeO}{100} \right) \qquad 2\text{-}22$$

Regarding to the slag viscosity, since it is dependable of the composition of the slag, the temperature and the partial pressure, its calculation is a complex task. Several empirical and semi empirical models were created to determine this property based on the chemical composition (V. Sinelnikov, 2015). The most popular models to estimate viscosity at the temperature range of 1400 -1700 °C for multicomponent systems are the Riboud and Urbain models (Appendix A).

In order to define the appropriate foaming conditions in the slag, some authors stablished correlations to calculate the foaming index Σ with a number of certain variables involved in the phenomena. The first relationship for foaming index Σ in aqueous foams related volume of the foam at steady state V_f and the gas flowrate blown Q_g (Bikerman, 1938), Equation 2-23:

$$\Sigma = \frac{\dot{\forall}_f}{Q_g} \qquad\qquad 2\text{-}23$$

Since Σ has units of time, it can be considered as the residence time of the bubbles in the foam (Jiang and Fruehan, 1991; Morales *et al.*, 2002). From the last Equation, a similar relationship was performed (Jiang and Fruehan, 1991), where the foaming index was defined by the ratio of the foaming height H_f (cm) and the superficial gas velocity V_g^s (cm/s), subsequently the result of dimensional analysis of H_f, V_g^s, ρ, μ and σ is reflected in Equation 2-24. These authors concluded that foaming increases by increasing the viscosity, and it decreases by increasing the surface tension.

$$\Sigma = \frac{H_f}{\overline{V}_g^s} = \frac{570 \cdot \mu}{\sqrt{\sigma \cdot \rho}} \qquad\qquad 2\text{-}24$$

From this correlation, the bubble diameter d_b was added to dimensional analysis (Zhang and Fruehan, 1995), obtaining the Equation 2-25

.

$$\Sigma = \frac{115 \cdot \mu^{1.2}}{\sigma^{0.2} \cdot \rho \cdot d_b^{0.9}}$$

2-25

Likewise, for bubble diameter for slags, some correlations were developed (Hesketh, Etchells and Russell, 1991) as shown in Equation 2-26:

$$d_s = \left(\frac{We_{crit}}{2}\right)^{0.6} \cdot \left[\frac{\sigma^{0.6}}{(\rho_c^2 \cdot \rho_d)^{0.2}}\right] \cdot \epsilon^{-0.4}$$

2-26

Where We_{crit} is the critical Weber number, the subscripts c and d are referred to continuous (slag) and dispersed (bubbles) phase.

Based on Equation 2-25, other physical model of slag foaming was proposed by adding the term of effective elasticity (E_{eff}) or surface tension depression (Ghag, Hayes and Lee, 1998), which is a function of the change in surface tension and the change of surface area (Equation 2-27). Thus, the resulting foaming index is expressed by Equation 2-28.

$$E_{eff} = \frac{A \cdot d\sigma}{dA} = \frac{d\sigma}{d\,LnA}$$

2-27

$$\Sigma = 1 \times 10^6 \cdot \left[\frac{\mu \cdot E_{eff}}{(\rho g)^2 d_b^3}\right]$$

2-28

Where *A* is the interfacial area and *g* is the gravity. From the experimental observation of these authors, they determined that bubble residence time increasing is more influenced by increasing of viscosity and decreasing of surface tension depression (E_{eff}) than by the decreasing of surface tension and decreasing of bubble time.

A practical model was developed considering the transient generation rate of CO during the process of a heat, this resulted in the concept of dynamic foaming index Σ_D (Morales *et al.*, 2002). To apply this approach, first it is necessary to define the foaming ratio $f_{r(t)}$ (Equation 2-29):

$$f_{r(t)} = \frac{\dot{\forall}^{sl}_{g(t)}}{\dot{\forall}_{sl(t)}} \qquad \text{2-29}$$

Where $\dot{\forall}^{sl}_{g(t)}$ is the volume rate of the gas plus slag and $\dot{\forall}_{sl(t)}$ is the volume rate of the slag production only. Their corresponding expressions are Equation 2-30 and 2-31:

$$\dot{\forall}^{sl}_{g(t)} = \frac{d\forall_{CO}}{dt} + \dot{\forall}_{sl(t)} \qquad \text{2-30}$$

$$\dot{\forall}_{sl(t)} = \frac{1}{\rho_{slg}} \cdot \frac{d\forall_{sl}}{dt} \qquad \text{2-31}$$

The first right-hand side term of the Equation 2-30 refers to the CO generation rate; the slag density ρ_{slg} of the Equation 2-31 can be obtained by Equation 2-21 and $\frac{d\forall_{sl}}{dt}$ represents the mass change of slag in the time. Then the dynamic foaming index Σ_D was determined by the product of the foaming ratio and the foaming index, Equation 2-32.

$$\Sigma_D = f_r \cdot \Sigma \qquad \text{2-32}$$

Chapter III

Methodology

The development of this work required of a sequence of steps (Figure 3.1), whose description is explained below.
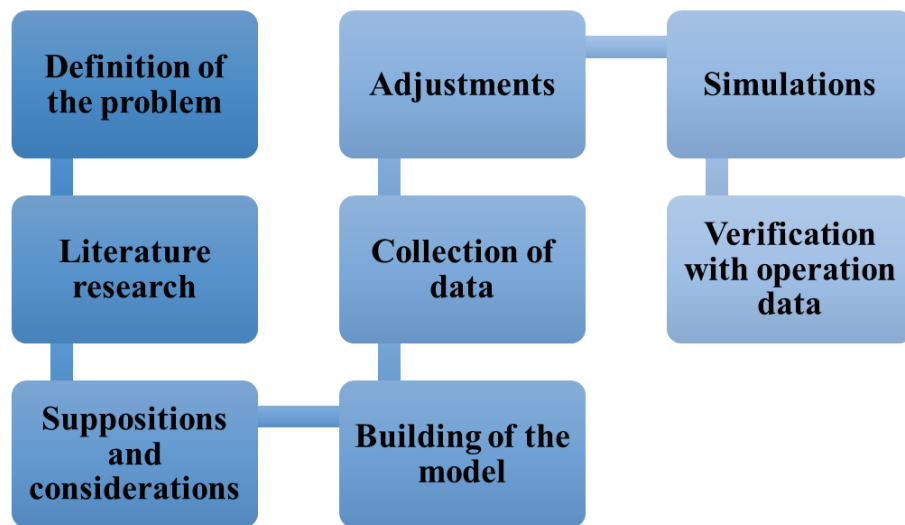
Figure 3.1 Sequence for the development of the mass and energy balance with transient approach.

1. **Definition of the problem and objectives.** This first step consisted on the meetings with the advisors to set the guidelines for the development of the model, the scope of the problem (delimitation), the objectives and the opportunities areas. This step is established in the first chapter of this thesis.

   Besides, some visits were made to steel mill with the aim of being familiarized with the EAF operation, this was an opportunity to learn about the process of a heat, the steps and the operative times, as well as to identify the available information and the limitations.

The important variables were identified: the inlets material flows, the chemical analysis of some inputs, the temperature of the inlets, the temperature of the hot heel, the temperature of the metal bath and the chemical analysis of the slag. But also, some data were unavailable such as composition of gases, infiltrations, volume of off gases and their temperature since the furnace was not completely instrumented.

2. **Literature research.** To have the proper basis to structure the model, the pertinent searching was made in research databases, thesis, institutional web pages, conference articles and books. For this case, the most relevant information was about EAF types and operation, models for mass and energy balance, chemical mechanisms for metallurgical process, chemical kinetics, slag foaming and chemical equilibrium. Some literature were defined as the most important (Bekker, Craig and Pistorius, 2000; Richard D. M. MacRosty, 2005; Trejo, 2012)(Morales *et al.*, 1995, 1997; Bekker, Craig and Pistorius, 1999; Richard D. M. MacRosty, 2005; Treviño, 2012) because of their objectives (similar to this work). This part is reflected in chapter II.

3. **Suppositions and considerations.** From the exhaustive research, it was possible to have the applicable basis and considerations for this work. The suppositions were made according to the available information for this EAF, the previous works and the scheduled time to finish this thesis research.

4. **Building of model.** The structuring of the model was carried out in the mathematical tool MATLAB®. The principal algorithm modules of the model are:

- Addition of mass and power flows profiles.
- Rate of scrap melting.
- Chemical kinetics. Estimation of the composition of each component at any time.
- Residence time of bubbles of CO and CO_2.
- Chemical equilibrium of gases.
- Slag spillage.

- Continuous inlets and outlets of gases.

5. **Collection of data.** Relevant data was requested to operation staff: material and energy addition profiles, amount of scrap, final production of steel, chemical analysis of materials (DRI, dolime, graphite), temperatures at flat bath conditions, temperature of inlet materials, Tap-to-Tap time, amount of hot heel, slag chemical analysis.

6. **Adjustment of the model.** With some data, the model was adjusted with some factors to deliver more accurate results, this is justified with the fact that some data is not available.

7. **Simulations and verification of the model:** Once having the adjustments for the EAF, some simulations were performed to compare the estimations of the model with the operation data. Also, to test the reliability of the model, a sensitive analysis was made.

The equipment employed was computer with the following features: operating system Windows 10, processor AMD A10-9600P RADEON R5, 10 compute cores 4C+6G 2.40 GHz, RAM disk of 12 GB and 1TB of available space in hard disk. These features are greater than those of the minimum requirements for MATLAB® (64-bits) software.

3.1 Assumptions and considerations

According to the actual limitations, the available data and the scientific basis, the following assumptions and considerations were made for this model in the EAF.

I. Transient state.

II. To enable the analysis of inherent phenomena, the system was divided in 4 main zones, as shown in Figure 3.2 (description at the first stage of the heat).

1. Gas zone. At the beginning of the process this comprises of air only, then the combustion reactions take place there, as well as it receives CO and CO_2 from slag zone. The chemical species considered for gas zone were: Methane CH_4, water H_2O, Hydrogen H_2, Nitrogen N_2, Nonane C_9H_{20}, Carbon monoxide CO, Carbon dioxide CO_2 and Oxygen O_2.

2. Slag zone. It is formed by a mixture of oxides, some additions (e.g. graphite, lime) and bubbles of CO. The chemical species considered for the slag zone are: Carbon monoxide CO, Carbon dioxide CO_2, Carbon C, Iron oxide FeO, ferric oxide Fe_2O_3, Silicon dioxide SiO_2, aluminum oxide Al_2O_3, Calcium oxide CaO, Magnesium oxide MgO, Manganese oxide MnO and titanium oxide TiO_2.
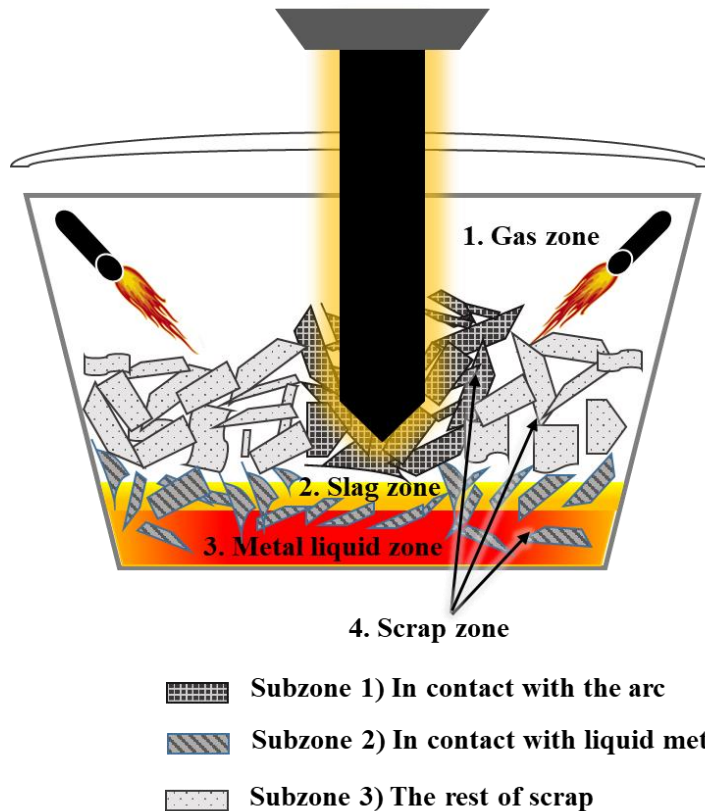
Figure 3.2 Schematic representation of an DC EAF (Initial stage).

3. <u>Liquid metal zone.</u> The amount of liquid steel depends on the power, the melting of scrap and the DRI addition, besides the rate of reduction reactions. By the lancing of oxygen here, the oxidation and decarburization reactions take place. The participant species for this zone are: oxygen O_2, Carbon C, Iron Fe, Silicon Si, Aluminum Al and Manganese Mn .

4. <u>Scrap zone.</u> In this zone, the 3 types of heat transfer mechanisms contribute for the scrap melting, to ease their analysis, this zone was distributed in 3 subzones: Subzone 1) the scrap in contact with the arc, Subzone 2) the scrap in contact with liquid metal/slag and Subzone 3) the rest of scrap.

III. 21 species in total were considered. The species with concentration with less than 0.1 wt. % were neglected (e.g. P_2O_5, S and Cr_2O_3), since their interaction do not provide a significant change of enthalpy. The nonane was used to represent the volatile components in the scrap as used in previous works for TMEB (Bekker, Craig and Pistorius, 1999; Richard D. M. MacRosty, 2005; Vito Logar and Skrjanc, 2012c).

IV. The addition profiles of materials and power from the arc were input, and the infiltrations and the off gases and the slag spillage were estimated. The profiles are programmed by operation protocols for each type of steel. According to the operation of this DC EAF, the addition profiles considered 13 principal inlet material flows: 1) scrap, 2) anthracite, 3) anthracite in scrap load, 4) graphite, 5) cold DRI (300.15 K), 6) hot DRI (593.15 K), 7) dolime, 10) Oxygen lance, 11) Oxygen burners, 12) water in the load and 13) air infiltrations.

V. The amount of liquid steel and slag that remains between the heats (hot heel) was considered. For this work, about 40 Ton of hot heel were employed, with a composition of 20% of slag and 80% of liquid steel. The purpose of this practice is to apply initial energy to the scrap before switching on the power (Morales *et al.*, 1995).

VI.   Just the reactions which provide or subtract meaningful energy were considered: Oxidation (Equations 2-11), decarburization (Equation 2-12), reduction (Equation 2-13 and 2-15), regeneration of *CO* (Equation 2-14) and combustion (burners).

VII.   It was assumed that the slag zone and the liquid metal zone are at the same temperature ((Bekker, Craig and Pistorius, 1999).

VIII.   The oxygen lances impact directly into the liquid metal zone. The products considered from the oxidation are the *FeO* and the *CO* only. According to experimental observations, *FeO* is transferred immediately to the slag zone (Bekker, Craig and Pistorius, 1999).

IX.   It was assumed that DRI pellets were melted instantaneously due to their simple geometry and size (8 mm), besides the maximum flow is added when the superheating occurs.

X.   According to some experiments and simulations with different graphite particle sizes for the reduction kinetics (Morales *et al.*, 1997), from the total amount of graphite added, just a certain fraction is able to enter to slag zone (f_c, carbon distribution). It is justified by the observation of the slag spillage through all the heat, and by the studies about the effects of solid flows, particle sizes, jet angles, momentum transfer and basicity of the slag on the entrained fraction of the graphite (Morales *et al.*, 1997). According to experimental data, operation conditions and slag properties the distribution factor is 0.6. The rest of the carbon fraction is either combusted at the surface or transported towards the continuous spillage.

XI.   To estimate the reaction rate in different zones these methods were used: kinetics for the slag and liquid metal zones, and chemical equilibrium for the gas zone.
Although previous works have employed chemical equilibrium for reactions in all zones (Richard D. M. MacRosty, 2005), in this model for practical purposes, time and computational resources savings, the chemical kinetics approach is applied. In contrast, for the gases zone the chemical equilibrium is almost instantaneous, so this method is more feasible.

XII.   Even though most of the composition of the Direct Reduction Iron (DRI) is Fe, some of its components (in less percentage) are oxides which are transferred to the slag zone. For that reason, a classification for mass transference was made:

- Species from DRI to the slag zone: $FeO, Fe_2O_3, SiO_2, Al_2O_3, CaO, MgO, MnO$ and TiO_2.
- Species from DRI to zone 3): C, Fe, Si, Al and Mn.

3.2 Elements for the structure of the model

The analysis of the EAF flows (before the tapping) was handled as a control volume, since the material is transferred through the boundaries continuously as shown in Figure 3.3. The inlet flows (mass and energy) are represented by the material additions ($\dot{m}_{in}h_{in}$) and the air infiltrations ($\dot{m}_{inf}h_{inf}$); the outlet flows (mass and energy) are represented by the off gases ($\dot{m}_{og}h_{og}$) and the slag pot ($\dot{m}_{slgd}h_{slgd}$). The heat in transit Q are represented by the energy from the arc ($\dot{E}$, inlet), the cooling system (outlet) and surroundings (outlet).
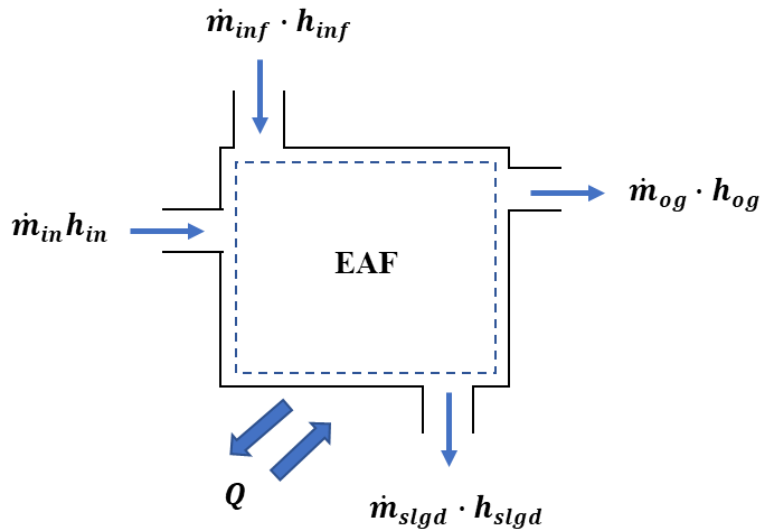
Figure 3.3 EAF control volume.

Inf: *Infiltrations,* ***in:*** *inlets,* ***out:*** *outlets,* ***slgd:*** *slag pot,* ***og:*** *off gases.* ***ṁ:*** *mass flow,* ***h:*** *enthalpy,* ***Q:*** *heat in transit.*

Once the boundaries were defined, and considering a non-steady state process with chemical reactions, the general mass and energy accumulation expressions were established by the Equation 3-1 and the Equation 3-2 respectively.

$$\frac{dM_{ij}}{dt} = \sum_{i=1}^{S} \dot{m}_{in_{ij}} - \sum_{i=1}^{S} \dot{m}_{out_{ij}} + \sum_{i=1}^{S} \dot{r}_{rxn_{ij}}$$

3-1

$$\frac{dE_{ij}}{dt} = \sum_{i=1}^{S} Q_{ij} - \sum_{i=1}^{S} \Delta H_{ij}$$

3-2

The subscripts i and j represents the zones and species; $\dot{m}_{in}$ and $\dot{m}_{out}$ are the inlet and outlet mass flows; $\dot{r}_{rxn}$ are the resultant mass of products and reactants consumption from the reactions. ΔH_{ij} is the total enthalpy in which the difference between outlets and inlets of energy for any zone are included, simultaneously this term represents the sensible heat $\int cp_j \cdot dT$, the energy from the reactions and the heat of phase change ΔH_{p1-p2}. For instance, the total specific enthalpy of liquid iron at a certain temperature T_{liq} is shown in Equation 3-3, this consist of several phase changes before reaching the melting point (from α to δ).

$$\widehat{H}°_{T_{Fe}}(T_{liq}) = \int_{298}^{1033} cp_{Fe_\alpha} dT + \Delta\widehat{H}_{\alpha-\beta} + \int_{1033}^{1187} cp_{Fe_\beta} \, d + \Delta\widehat{H}_{\alpha-\gamma}$$

3-3

$$+ \int_{1187}^{1665} cp_{Fe_\gamma} dT + \Delta\widehat{H}_{\gamma-\delta} + \int_{1665}^{1809} cp_{Fe_\delta} + \Delta\widehat{H}_{\delta-liq} + \int_{1809}^{T_{liq}} cp_{Fe_{liq}} dT$$

Where C_P is the heat capacity at constant volume, this can be consulted in Table C.3.

For the comprehensive explanation of the energy balances for each zone, the schemes from the Figure D.1 and Figure D.2 can be consulted.

On the other hand, the structure of the mass and energy balance (MEB) model with transient approach is formed by modules for different phenomena and operate in different zones, their specifications are shown in the Figure 3.4. Each module is explained below with their corresponding zone, except for the cooling system, since it is just input as a profile of increments of temperatures, this data was obtained in plant along with the water flows in the panels.
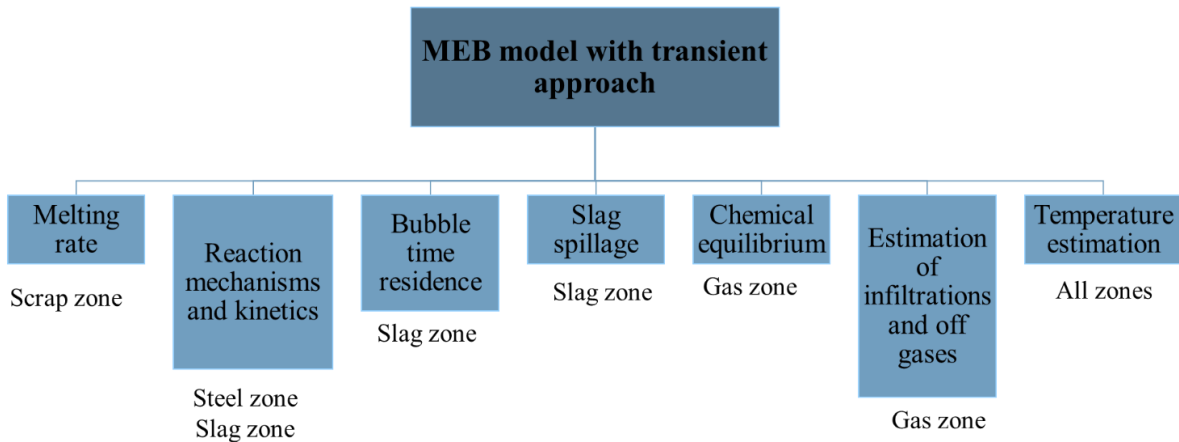
Figure 3.4 Block diagram of the modules of the MEB model with transient approach.

3.2.1   Structure of the melting rate module

First, the scrap domain was divided in 3 subzones according to their different heat transfer mechanisms as shown in Figure 3.5. For the modeling they were defined as follows, and their heat transfer expressions are defined in Table 3.1, where the thermal conductivity factors K and the convection factors h have implicit the values of surfaces and lengths.

- Subzone 1) Scrap in contact with the radiation. The entrance of heat is via radiation and the exit is by the heat conduction with nearby pieces of subzone 3).

- Subzone 2) Scrap in contact with the liquid metal. The inlet of heat occurs by convection from liquid metal zone to scrap pieces, while the outlet of heat is done by conduction with pieces of subzone 3).

- Subzone 3) The rest of scrap. The inlet of heat is due to the outlets from the previous subzones, besides the energy from the flames (according to the placement of the burner for this furnace). The outlet of heat from this subzone is transferred to gas zone.

Then, a distribution for the size of subzones was made: 10% for subzone 1), 10% for subzone 2) and 80% for subzone 3). The general expression to determine the actual energy content in each subzone at any time consisted in the sum of the enthalpy at the previous step of time and the heat transfer balance, Equation 3-4.

Where S_{sz} is the size distribution of the subzone, H_{sz}^{t-1} is the energy accumulation from previous step for scrap zone.

$$H_{sz} = S_{sz} \cdot H_{sz}^{t-1} + (\dot{Q}_{in_{sz}} - \dot{Q}_{out_{sz}}) \hspace{2cm} \text{3-4}$$
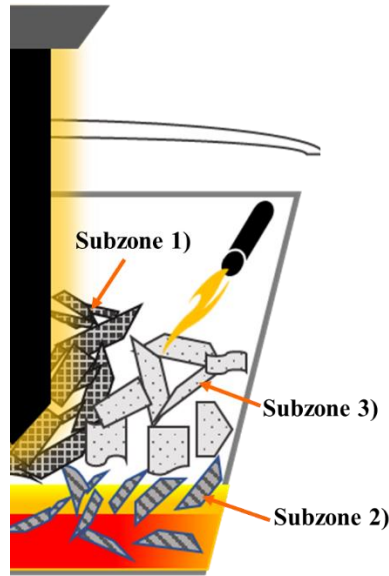
Figure 3.5 Subzones of the scrap zone.

Afterwards, the molten mass for each subzone and the remaining energy are determined by setting the fusion heat (at 1809 K) as constraint. In this case, if the energy content of the subzone exceeds

Table 3.1 Heat balance in subzones.

Subzone	Inlet/outlet	Expression and value of the factors
Subzone 1) Scrap in contact with the arc	Inlet heat: **Radiation**	$\dot{Q}_{in_{sz1}} = P_{arc} \cdot VF_{sz1}$
	Outlet heat: **Conduction to Subzone 3)**	$\dot{Q}_{out_{sz1}} = K_{sz1-sz3} \cdot \Delta T_{sz1-sz3}$ $K_{sz1-sz3} = 1000\dfrac{W}{K}$
Subzone 2) Scrap in contact with the liquid metal	Inlet heat: **Convection from metal liquid zone**	$\dot{Q}_{in_{sz2}} = h_{mm} \cdot \Delta T_{mm-sz2}$ $h_{mm} = 1300\dfrac{W}{K}$
	Outlet heat: **Conduction to Subzone 3)**	$\dot{Q}_{out_{sz2}} = K_{sz2-sz3} \cdot \Delta T_{sz2-sz3}$ $K_{sz2-sz3} = 400\dfrac{W}{K}$
Subzone 3) The rest of the scrap	Inlet heat: **Outlet heat from Subzones I) and II) and flames**	$\dot{Q}_{in_{sz3}} = \dot{Q}_{out_{sz1}} + \dot{Q}_{out_{sz2}} + \dot{q}_0 e^{-\beta x}$
	Outlet heat: **Convection to zone 1)**	$\dot{Q}_{out_{sz3}} = h_{gas} \cdot \Delta T_{sz3-gas}$ $h_{gas} = 98.88\dfrac{W}{K}$

P_{arc}: Power flow (MW), VF_{sz1}: View factor from the arc to the scrap, K:Thermal conductivity factor (W/m·K), $\Delta Tszi$-szj or zj: Differential of temperatures between subzones or subzone-zone, h_{mm}: Liquid metal heat transfer factor(W/K), h_{gas}: Gases heat transfer factor (W/K), $\dot{Q}_{in}$: Inlet heat y $\dot{Q}_{out}$: Outlet heat, q_0= Heat flow supplied by the flame, β:Damping factor of the flame and x: vertical coordinate of the flame.

the fusion heat, as a result, the fusion of the scrap occurs. And last, the total melting rate is determined by the sum of molten scrap from each subzone respect to time, as consequence, the scrap zone gradually disappears, and the liquid metal zone increases. After all the scrap zone disappears the power flow from the arc is supplied directly to the steel until flat bath conditions (about 1896 K) are reached.

3.2.2 Chemical kinetics structure

According to the reviewed reaction mechanisms in the literature (Jiang and Fruehan, 1991; Morales *et al.*, 1997; Richard D. M. MacRosty, 2005) and some considerations (subsection 3.1), a combination of these reactions were taken for the metal liquid zone and slag zone.

- Metal liquid zone: Oxidation (Equation 2-11) and decarburization (Equation 2-12). The FeO and the gaseous CO (as bubbles) produced are transferred instantaneously to slag zone.

- Slag zone: A schematic representation of the slag mechanism is shown in Figure 3.6, where all reactions are endothermic, consequently they may decrease the bath temperature. Here the availability of the CO bubbles depends on their residence time, as they enter, the nucleation occurs, and the graphite particles are trapped by them. To simulate the effect of silicon dioxide (Morales *et al.*, 1997), Equation 3-5 was applied in this module.

$$\theta_{SiO_2} = 0.378784 - 0.43079 \left(\frac{wt.\% \, FeO}{100} \right) + 0.614993 \cdot a_{siO_2} \qquad \text{3-5}$$
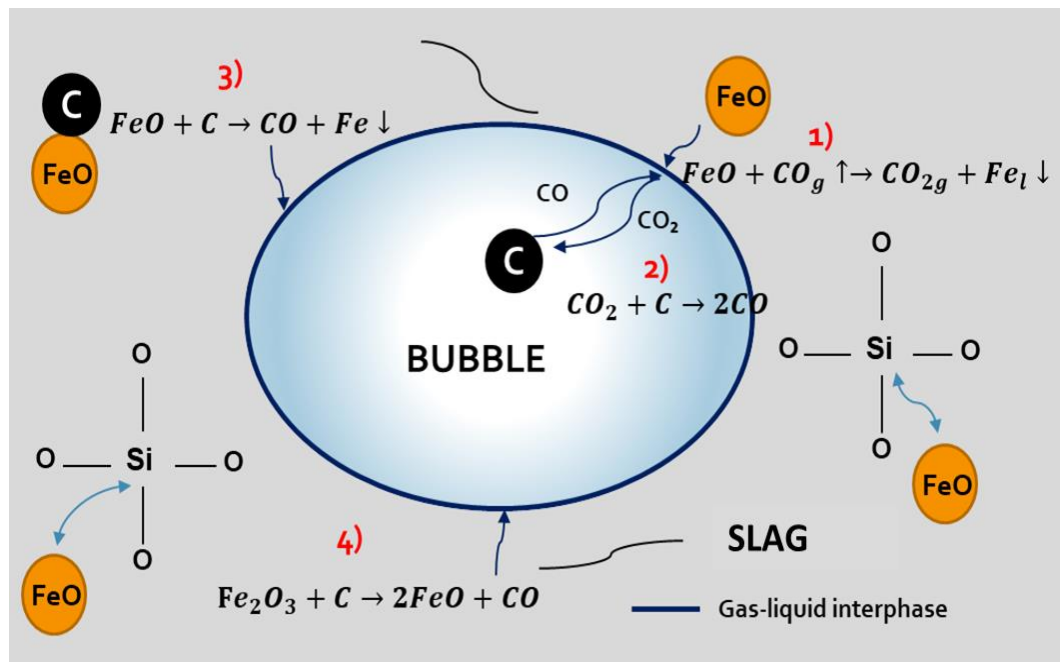
Figure 3.6 Proposed reaction mechanism within the slag zone.

Where θ_{SiO_2} is the unavailable surface for FeO and a_{siO_2} is the activity of the silicon dioxide.

1) Once FeO reaches CO bubble surface, the reduction (Equation 2-13) occurs, producing CO_2 and Fe. Last one is transferred to liquid metal zone.

2) Carbon monoxide is regenerated by Boudouard's reaction (Equation 2-14) by the contact of CO_2 and graphite particles C.

3) Simultaneously, Carbon particles can reduce FeO (Equation 2-15) directly, obtaining more stable CO bubbles (Zhang and Fruehan, 1995).

4) Because of the content of hematite Fe_2O_3 in the DRI, it is also reduced by carbon particles, having more contribution of FeO and CO

$$Fe_2O_3 + C \rightarrow 2FeO + CO \qquad\qquad \text{3-6}$$

The reaction rate of each component (*j*) was estimated by the general Equation 3-7:

$$\frac{dc_j}{dt} = \left(k1 \cdot c_k - k_2 \cdot c_j \cdot c_l \right) \qquad\qquad \text{3-7}$$

Where k_n is the rate constant for a given reaction, c_i corresponds to the specie mole-concentration, and dt is the differential of time. The positive sign refers to generation and the negative sign refers consumption. The rate constants k for the set of reactions were found at databases (Westley, 1980; National Institute of standards and technology, 2017) and articles:(Philbrook and Kirkbride, 1956; Rao, 1971; Sain and Belton, 1976), according to these records, the set of reactions from above are stablished as elemental. This kinetics data was employed to observe the behavior of the mechanism, but high instability was observed, due to this limitation, the method to obtain k values was semi statistical from the adjustments of several heats data.

The detailed kinetic models for the steel zone and slag zone are described in the Table 3.2 and Table 3.3 for each specie (reactant or product), where the units of the concentrations c_j are given by $\frac{mol}{cm^3}$ and the units of the kinetic equations are given by $\frac{mol}{cm^3-s}$ (concentration/time).

Table 3.2 Kinetic model for the liquid steel.

Velocity constants	**Kinetic equations per specie $\frac{mol}{cm^3-s}$**
$k_{s1} = 0.85 \dfrac{cm^{1.5}}{mol^{0.5} \cdot s}$ $k_{s2} = 0.37 \dfrac{cm^{1.5}}{mol^{0.5} \cdot s}$	$\dfrac{dN_C}{dt} = -k_{s1} \cdot c_C \cdot c_{O_2}^{0.5}$ $\dfrac{dN_{O_2}}{dt} = -k_{s1} \cdot c_C \cdot c_{O_2}^{0.5} - k_{s2} \cdot c_{Fe} \cdot c_{O_2}^{0.5}$ $\dfrac{dN_{Fe}}{dt} = -k_{s2} \cdot c_{Fe} \cdot c_{O_2}^{0.5}$ $\dfrac{dN_{CO}}{dt} = k_{s1} \cdot c_C \cdot c_{O_2}^{0.5}$ $\dfrac{dN_{FeO}}{dt} = k_{s2} \cdot c_{Fe} \cdot c_{O_2}^{0.5}$

$\boldsymbol{k_{s1}}$ = *velocity constant for the reaction 2-12,* $\boldsymbol{k_{s2}}$ =*velocity constant for the reaction 2-11 and* $\frac{dN_j}{dt}$ = *velocity of change of moles per specie.*

After the estimation of the changes for each specie, it is important to consider the mass transfer from the slag zone to the gas zone (determined by residence time bubbles) and from the slag zone to the metal zone. With the mass remaining, a profile of compositions (% Wt.) was built to ease the comparison with real analysis of slag.

Table 3.3 Kinetic model for the slag.

Velocity constants	Kinetic equations per specie $\frac{mol}{cm^3-s}$
$k_1 = 6.4 \times 10^2 (1 - \theta_{SiO_2}) \frac{cm^3}{mol \cdot s}$	$\frac{dN_{Fe}}{dt} = k_1 \cdot c_{FeO} \cdot c_{CO} + k_3 \cdot c_{FeO} \cdot c_C$
$k_2 = 9.36 \times 10^2 \frac{cm^3}{mol \cdot s}$	$\frac{dN_C}{dt} = -k_2 \cdot c_C \cdot c_{CO_2} - k_3 \cdot c_{FeO} \cdot c_C - k_4 \cdot c_{Fe_2O_3} \cdot c_C$
$k_3 = 6.5 \times 10^2 \frac{cm^3}{mol \cdot s}$	$\frac{dN_{FeO}}{dt} = -k_1 \cdot c_{FeO} \cdot c_{CO} - k_3 \cdot c_{FeO} \cdot c_C + 2 \cdot k_4 \cdot c_{Fe_2O_3} \cdot c_C$
$k_4 = 6.1 \times 10^2 \frac{cm^3}{mol \cdot s}$	$\frac{dN_{CO}}{dt} = -k_1 \cdot c_{FeO} \cdot c_{CO} + k_3 \cdot c_{FeO} \cdot c_C + 2 \cdot k_4 \cdot c_{Fe_2O_3} \cdot c_C$
	$\frac{dN_{CO_2}}{dt} = k_1 \cdot c_{FeO} \cdot c_{CO} - k_2 \cdot c_C \cdot c_{CO_2}$
	$\frac{dN_{Fe_2O_3}}{dt} = -k_4 \cdot c_{Fe_2O_3} \cdot c_C$

$k_{1,2,3,4}$= *velocity constant for the reaction 2-13 to 2-15 and*, $\frac{dN_j}{dt}$ = *velocity of change of moles per specie*, θ_{SiO_2}= *the unavailable surface for FeO.*

3.2.3   Bubbles residence time: structure

To determine the CO-bubbles residence time in the slag zone, the criteria of the dynamic foaming index (Morales *et al.*, 2002) was applied. The foaming ratio was estimated by the Equations 2-29, 2-30 and 2-31; the static foaming index by Equations 2-27 and 2-28, and the dynamic foaming index by 2-32.

The estimation of slag properties was calculated by empirical correlations:

- Slag density ρ_{slag}: Equation 2-21.
- Surface tension σ: Equation 2-22.
- Bubble diameter D_b: Equation 2-26.
- Viscosity μ: model of Urbain (Appendix A).

To establish the dynamic times of residence times in accordance with the CO generation, and its transference from slag zone to gas zone, the following arrangement was applied (Equation 3-8).

$$\frac{dN_{CO}}{dt} = N_{CO_{in}} - N_{CO_{out}}$$

3-8

Where $\frac{dN_{CO}}{dt}$ is the change of moles per unit time, $N_{CO_{in}}$ is the CO inlet molar flow (mole/min) which enters from metal liquid zone to slag zone, and $N_{CO_{out}}$ is CO outlet molar flow which escapes to gas zone.

3.2.4 Gases equilibrium structure

Since the reactions in the gas zone reach very fast the thermodynamic equilibrium, the method of minimization of Gibbs free energy was employed here (White, Johnson and Dantzig, 1958). For the hypothetical conditions inside the furnace, the activities coefficients $\gamma = 1$, and the existing species are $CH_4, H_2O, H_2, N_2, C_9H_{20}, CO, CO_2$ and O_2.

For the implementation of this procedure, first, the standard Gibbs free energies $G_j°$ were determined for each specie (Table C. 2) and a matrix of atomic balance A_{eq} (Equation 3-9) was built. Where the rows represent the elements and the columns the species. Subsequently, B_{eq} (Equation 3-9) was estimated by the product of A_{eq} and N_{eq} (available moles of the participant species).

$$A_{eq} = \begin{matrix} CH_4 & H_2O & H_2 & N_2 & C_9H_{20} & CO & CO_2 & O_2 \\ \begin{bmatrix} 0 & 1 & 0 & 0 & 0 & 1 & 2 & 2 \\ 1 & 0 & 0 & 0 & 9 & 1 & 1 & 0 \\ 4 & 2 & 2 & 0 & 20 & 0 & 0 & 0 \\ 0 & 0 & 0 & 2 & 0 & 0 & 0 & 0 \end{bmatrix} & \begin{matrix} Oxygen\ balance \\ Carbon\ balance \\ Hydrogen\ balance \\ Nitrogen\ balance \end{matrix} \end{matrix}$$

3-9

3-10

$$B_{eq} = A_{eq} \times N_{eq}$$

The optimization technique of interior point (algorithm fmincom from MATLAB®) was employed to minimize the free Gibbs energy until the equilibrium is reached in each step of time.

3.2.5 Estimation of continuous spillage of slag

To avoid the excess of slag accumulation, the furnace has an outlet door, which is useful when the contents of slag exceed the maximum height at specific level, then it drains into a short channel, and is spilled towards a slag pot. To determine this outlet of mass the following steps were structured in the modeling.

First, the slag zone and the metal zone volumes were calculated by their densities values, the sum of both represents the furnace content. To determine the maximum volume and the maximum height at slag door level, the structural plans of the furnace were employed. For this case, maximum volume and height up to the slag door are 28.2762 m^3 and 1.2491 m respectively, being the last one the constraint of mass outlet.

The outlet volume of slag is the difference of the furnace content and the maximum volume:

$$\forall_{outlet} = \forall_{Total} - \forall_{Max} \qquad\qquad 3\text{-}11$$

After the level of the slag door, the geometry begins as a regular cylinder, so, the height above this level is calculated by Equation 3-12, considering that a tiny amount of slag exceeds the maximum height.

$$H_{above} = \frac{\forall_{outlet}}{A_{T_{sd}}} \qquad\qquad 3\text{-}12$$

Where $A_{T_{sd}}$ is the transversal area after the slag door level.

The outlet slag mass flow or spillage flow $\dot{m}_{out}$ was obtained by Equation 3-13. The gravity is g, and A_{ch} is the drain channel area.

$$\dot{m}_{out} = \frac{\left(\sqrt{2 \cdot g \cdot H_{above}}\right)}{A_{ch}} \cdot \rho_{slag} \qquad \text{3-13}$$

3.2.6 Estimations of air infiltration and off gases

The estimations of the air infiltrations and the off gases depend on two factors: the available volume in the EAF and the extraction flow of the chimney. The available volume $\forall_{av}$ was determined by the difference between the total volume of the EAF $\forall_{To}$ and the contents $\forall_{mix}$ (metal liquid and slag), this was employed as main constraint.

$$\forall_{av} = \forall_{To} - \forall_{mix} \qquad \text{3-14}$$

The actual volume of gases in each step of time was defined by the difference of volume after equilibrium V_{gT} and the volume extracted by the chimney $\forall_{chim}$ (Equation 3-15). Since the volumetric flow of extraction for this furnace is not monitored, an estimate an approximation was used for the calculation of the off gases, using as reference some literature data (Kirschen, Velikorodov and Pfeifer, 2006).

$$\forall_{gas} = \forall_{gT} - \forall_{chim} \qquad \text{3-15}$$

In the case in which the actual volume of gases is lower than the available volume, this volume missed is replaced by the air infiltrations, which were defined by Equation 3-16.

$$\forall_{inf} = \forall_{av} - \forall_{gas}$$

<div align="right">3-16</div>

Once having the volume of infiltrations, the mole amount can be obtained using the environment pressure, the temperature and the air composition. At each step of time the volume of gas in the furnace and its composition were calculated after the production of reactions and the infiltrations, therefore, these compositions are employed for the calculation of the off gases mass and the gas temperatures.

3.2.7   Estimation of Temperatures

Due to the transient approach, the estimation of temperature profiles (variable temperatures at each step of time) are needed to obtain the energies for each zone. Since the temperatures are not monitored during all the "heat, the solver for nonlinear equations *fsolve* (MATLAB®) was used to calculate the temperatures by the values of enthalpies and the incoming power, for this purpose, the following function (Equation 3-17) was employed, being T_{new} the unknown.

$$f(T) = H_{in} - \sum N_{out} \cdot h_{flow}(T_{new}) + Q$$

<div align="right">3-17</div>

H_{in} is the incoming enthalpy for any zone before reactions; N_{out} is the mole content at the end for each zone; h_{flow} is the function employed for enthalpy; T_{new} is the new temperature estimated and Q is the heat in transit.

As mentioned in the considerations, the temperature of liquid steel and the temperature of slag are the same. As the main inlet in this zone is the energy from the arc, it is important to mention that this is transferred to the surroundings by three ways in different percentages: electrons (3.5%),

convection (72.5%) and radiation (24%) (J. L. G. Sánchez, 2009), thus, the input heat of steel zone was handled by the Equation 3-18.

$$Q_{in,z3} = (1 - Loss_e) \cdot E_{arc} \cdot (\%Q_{conv} \cdot cov + \%Q_{elec} + \%Q_{rad} \cdot VF_{arc-z3}) \qquad \text{3-18}$$

Where $Loss_e$ is the electric losses portion (6%) , E_{arc} is the energy from the arc, $\%Q_{conv}$, $\%Q_{elec}$ and $\%Q_{rad}$ are the percentages of heat transfer, cov is the arc coverage and VF_{arc-z3} is the view factor from the arc to the liquid bath of 0.4033 (Trejo, 2012)). The outlet of heat occurs by the convection into the scrap (before all the scrap is molten) and the convection into the gas zone. For the estimation of gas zone temperature, the inputs of heat are the convection transfer from the hot scrap Q_{scr-z1} (during the process of fusion) and the heat transfer from the liquid steel Q_{ls-z1}, the rest of convection and the combustion energy Q_{comb}, as shown in Equation 3-19.

$$Q_{in,z1} = Q_{scr-z1} + Q_{ls-z1} + (1 - Loss_e) \cdot E_{arc} \cdot \%Q_{conv} \cdot (1 - cov) + Q_{comb}) \qquad \text{3-19}$$

Once having the first estimation of the profiles of gas temperatures, a recalculation was performed to improve the approximation by the addition of unrecognized losses. For this purpose, the following sequence was employed:

1. Calculation of the energy residual (difference between energy inlets and outlets).
2. Calculation of the fraction of addition (difference between residual energy and off gases energy).
3. Sum of the fraction of addition and the off gases energy.
4. Obtaining of specific enthalpy of the last sum.
5. Recalculation of gas temperatures based on the first estimation and the specific enthalpy calculated in the last step. Again, a solving was employed with the following function (Equation 3-20).

$$f(T) = E_{OG} - \sum N_{OG} \cdot (h_{flow}(T_{new}) - h_{flow}(T_{ref}) \qquad \text{3-20}$$

E_{OG} represent the energy of the off gases and N_{OG} the resulting moles of them.

3.2.8   Cooling system losses estimation

With the cooling system information from the steel mill, it is possible to know the different increment of temperatures ΔT during the heat, thus this profile is an input data for the model, as well as, the volumetric flows for the shell, roof and elbow (Figure B.2). The general energy losses in the cooling system is estimated by the Equation 3-21.

$$Q_{cs_T} = \rho_w \cdot C_{p_w} \cdot \Delta T \cdot \frac{\dot{\forall}_{shell} + \dot{\forall}_{roof} + \dot{\forall}_{elbow}}{dt} \qquad \text{3-21}$$

Where ρ_w is the density of water, C_{p_w} is the heat capacity of water at the entrance of the cooling system and $\dot{\forall}$ is volumetric flow.

3.3   Collection of data

The collection of operation data was supply by the personnel of the steel mill, to organize the requests, a checklist was made (Table B.1). To obtain a proper accuracy, several heats with similar "recipes" were analyzed to adjust the model.

First, since the dynamic data of additions were provided by accumulation of power, mass and volume, they were converted to flows and then they were plotted (Figure B.1, Figure B.2 and Figure B.3) to obtain the profiles, which enable the identification of the time ramps. For each ramp an average of power, mass or volumetric flow was calculated, in this way, this data was input into the model.

The slag sampling for this work was useful to corroborate the simulation of kinetics, however, for the personnel safety, just 4 samples per heat were taken after the 30 minutes, in intervals of 10

minutes approximately. It is worth to mention that at the time of the slag sampling the bath is almost homogeneous due to the fluid movement, so, it is considered that there is no significant variation of compositions. At laboratory the analysis of slag is determined by X-ray diffraction technique.

Other important data were:

- The amount of hot heel (40 Ton),
- The amount of tapped steel (145.45 Ton),
- Chemical analysis of some inputs (dolime, graphite and DRI),
- Chemical analysis of slag at the end of the heat,
- Temperatures of flat bath, (1907.5 K),
- Tap-to-Tap time (72 minutes).

3.4 Adjustments of the model

Due to several assumptions, some unavailable data and complexity of this system, some adjustments were needed. Along with the building of module structures, operation data from the literature was employed to determine initial adjustment factors which stabilized the results.

Once all the model was built, with initial factors several simulations were run for the same type of heat (1 D), some factors were discarded and some of them were modified to stabilize the system. In this case, due to the limitation of time and access to more operation data, the adjustments were made with 3 heats. The resulting adjustable parameters are showed in Table 3.4, where the main adjustments were carried out in the heat balances for scrap melting and in the kinetics. For the last ones, the initial values were obtained from databases and literature, and they were maintained fixed since the temperature among the heats are closed.

As one of the most important contributions of these model is the kinetic model, its reliability was tested of by a sensitive analysis, modifying the following input variables:

Table 3.4 Adjustable factors.

Factor	*Value*	Description
$K_{sz1-sz3}, K_{sz2-sz3}$	<u>1000</u>, <u>400</u> (W/K)	Heat transfer factors of conduction with implicit surface and length.
h_{mm}, h_{gas}	<u>1300</u>, <u>98.88</u> (W/K)	Heat transfer factors of convection with implicit surface.
ks_1, ks_2	<u>35.85</u>, <u>0.37</u> ($\frac{cm^{1.5}}{mol^{0.5} \cdot s}$)	Rate constants for reaction in the steel zone.
k_1, k_2, k_3, k_4	<u>6.4E2</u>, <u>9.36E2</u>, <u>6.5E2</u>, <u>6E2</u> ($\frac{cm^3}{mol \cdot s}$)	Rate constants for reactions in the slag zone.
$\dot{\forall}_{chim}$	<u>1312</u> ($\frac{m^3}{min}$)	Extraction volumetric flow.

*Suffixes. $sz1 - sz3$: from subzone 1 to subzone 3, $sz2 - sz3$: from subzone 2 to subzone 3, **mm**: between the liquid metal and subzone 2, **gas**: between the liquid metal and gas zone and **chim:** chimney.*

- The composition of carbon in DRI, where the actual concentration is 3.6% and it will be tested at 50% less and 50 % more of this value.
- The composition of iron oxide in DRI, where the actual concentration is 5% and it will be tested at 50% less and 50 % more of this value.

With the resulting profile of composition of iron oxide and carbon in the slag zone, 3 plots were built for 3 stages of the "heat": the ending of fusion, the intermediate time (50 minutes) and the end of the heat (72 minutes). The purpose of these graphics is to observe the deviation of the results for the behavior of the composition of CO in the slag. It should be noted that for a rigorous sensitivity analysis of the parameters a design of experiments is needed with more samples.
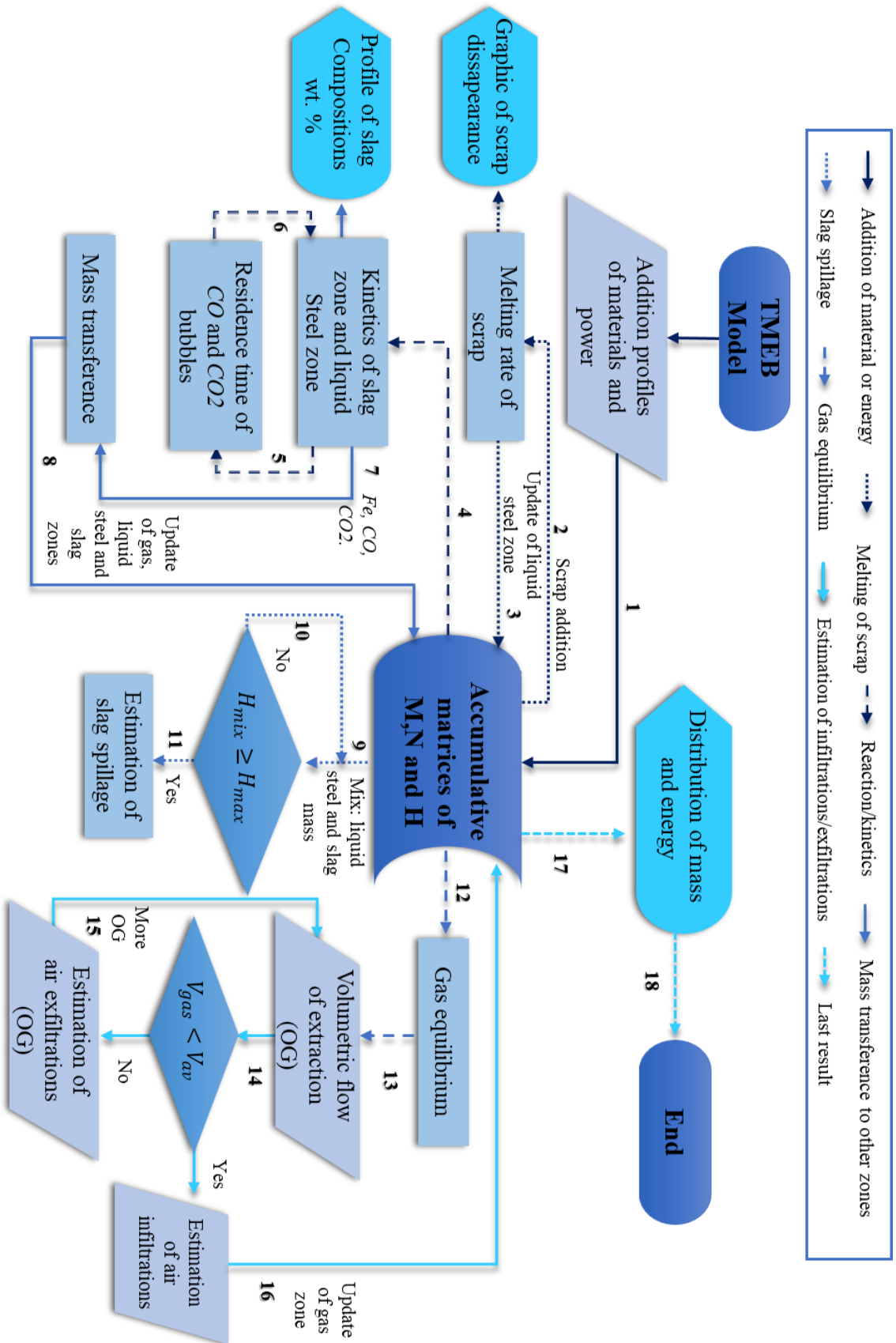
Chapter IV

Results

After the delimitation to characterize the system, the model was built in a numerical computing software, in this section, this structure is described since it is one of the most important results as such. Then, with the collection and analysis of new operation data and the adjustments, it was possible to perform some simulations, having as relevant results:

- Evolution of the melting of scrap.
- Chemical kinetics in the slag, displayed in compositions (Wt. %).
- Sensitive analysis before the change of composition of C and FeO in DRI.
- Mass distribution profiles
- Mass and energy distribution at any time.
- Temperature profiles for each zone.
- Final mass and energy balance.

4.1 Description of the MEB model with transient approach

This model was comprised of 7 main modules: the addition of material/energy, the melting of scrap, the steel-slag kinetics, the residence time of bubbles, the slag spillage, the gas equilibrium and the estimation of exfiltrations/infiltrations. The Figure 4.1 shows a flow chart of the specific structure and sequence of the model for a step of time (0.1 min), therefore, this process is repeated until the Tap-to-Tap time is over, in this case for 720 steps of time, since it is 72 min.

As can be observed, through all the sequence there are 3 matrices of accumulation of mass, mole and energy: M_{acum} (Ton), N_{acum} (mole) and H_{acum} (Joules), which are updated after any process

Figure 4.1 Flow chart of the MEB model with transient approach.

H_{mix}: Height of liquid steel an slag, H_{max}: Height up to the slag door, V_{av}: available volume in the EAF and V_{gas}: actual volume of gas. M, N and H :mole and energy respectively; **OG**: Off gases.

and save the information of each magnitude. These arrangements enable a flexible modeling, in fact, the zones are represented by the rows (*i*) and the chemical species by the columns (*j*). Similar to the Equation 3-1, the arrangement of the accumulative mass matrix is evaluated by Equation 4-1, where $M^{t-1}_{acum_{ij}}$ is the mass of the preceding time interval, M_{in} and M_{out} are the inlet and the outlet of mass. From this matrix, the mole matrix $N_{acum\ ij}$ is obtained by a conversion and molecular weights (PM_c) as shown in Equation 4-2.

$$M_{acum_{ij}} = M^{t-1}_{acum_{ij}} + M_{in_{ij}} - M_{out_{ij}}$$

4-1

$$N_{acum\ ij} = \frac{M_{acum\ ij} \cdot 1 \times 10^6}{PM_c}$$

4-2

With the employment of $N_{acum\ ij}$, the matrix of energy accumulation $H_{acum_{ij}}$ is obtained by Equation 4-3, using a function of Enthalpy ($\widehat{H}_T$) at any given temperature T_{ij}.

$$H_{acum_{ij}} = N_{acum_{ij}} \cdot \widehat{H}_{T_{ij}}(T_{ij})$$

4-3

It should be noted that this function was developed (Trejo, 2012) using the concept of Total Enthalpy, to calculate the actual energy, the enthalpy of formation was removed at the reference temperature of 298.15 K.

Continuing with the details of the sequence, as shown in Figure 4.1, its order was represented by numbers, and the cycles for each module or additional process (mass transference and last result) was delimited by different types of arrows (listed at the top of the flow chart).
As at the beginning of the heat, the gas zone comprises just of air, and the slag zone and the liquid metal zone of their composition percentages in the hot heel, this data is stored in the matrices of accumulation since the time zero. The general explanation of the flow chart is listed below.

Addition profiles of material and power. Subscript 1, arrows ➡

According to the consideration IV, there are 13 principal material flows and 1 of power flow (from the arc). This data is adapted to the model and discretized by time intervals of addition. Each stream has a corresponding vector of concentrations c_x ($wt.\%$) and a maximum flow $\dot{m}_{max}$, thus, the mass additions of the streams M_x (x was any stream) are defined by the Equation 4-4. Where f_x represents the fraction of maximum flow, and dt the differential of time.

$$M_x = \dot{m}_{max} \cdot c_x \cdot f_x \cdot dt \qquad\qquad 4\text{-}4$$

This data is input into the storage (matrices of accumulation) in each step of time (**1**, Figure 4.1), these flows are distributed to the corresponding zone with their magnitudes of mass or energy dynamically. For a practical handling the oxygen and natural gas volume flows are converted to mass flows. The selective mass transfer is made according to consideration XII at the time of addition.

Melting rate. Subscripts 2 and 3, arrows ⋯➤

After the addition of the basket (s) of scrap (**2**, Figure 4.1), the estimation for the melting rate of scrap is made by the power flow from the arc along with the heat transfer mechanisms for each subzone. As the scrap is gradually melted, this liquid mass is updated into the liquid metal zone (zone 3) in the storage (**3**, Figure 4.1), additionally, the graphic of scrap disappearance is displayed. It should be noted that after all the scrap is molten, the energy from the arc is allocated towards the liquid metal zone to reach flat bath conditions.

Reaction/kinetics. Subscripts 4, 5 and 6, arrows ‑➤

The velocities of the reactions are estimated on basis of the proposed reaction mechanisms for the liquid metal and the slag zones, and the additions of some reactants like oxygen lance and carbon (**4,** Figure 4.1). To determine the real volume occupied by the CO bubbles and the time availability to react, the model for the definition of residence time bubbles is employed (**5**, Figure 4.1), since CO is produced and consumed in the slag simultaneously, there is a double relationship in this zone in the inlet and outlet of bubbles (**6,** Figure 4.1).

Mass transference to other zones. Subscripts 7 and 8, arrows ➝

After the estimations of the velocities of reaction some products are transferred among the zones (**7,** Figure 4.1), the FeO and CO produced at the liquid metal zone are transferred to slag zone; the Fe recovered in the slag is transferred back to the liquid steel zone and the CO and CO_2 are transferred to the gas zone. As a result, a new distribution of the accumulative matrices is made by the updating among the zones (**8,** Figure 4.1). The immediate result from this module is the display of the profile of slag compositions %Wt. during all the steps of time.

Slag spillage. Subscripts 9,10 and 11, arrows ┄➤

By setting the volume occupied by the steel and the slag zone as the mix volume (**9,** Figure 4.1), the corresponding height is obtained by geometry and having as restriction the height up to the slag door, it can be determined whether there is slag spillage or not. In the case of not having spillage (**10,** Figure 4.1). the process is returned to the mix, and in the case of exceeding the slag door height (**11,** Figure 4.1), the estimation of the slag spillage takes place, and of course, this portion is taken out from the matrices of accumulation.

Gas equilibrium. Subscripts 12 and 13, arrows ┅➤

With the amount of the mass and energy from the volumetric additions and products from other zones (**12,** Figure 4.1) the velocity of reaction in the gas zone is obtained by the minimization of Gibbs free energy (equilibrium) taking the consideration XI and handling 8 gaseous species (**13,** Figure 4.1).

Estimation of infiltrations/exfiltrations. Subscripts 14, 15 and 16, arrows ➝

Once having the volume of gas from the equilibrium v_{gas} and introducing the data of the volumetric flow of extraction (**14,** Figure 4.1), the infiltrations of air and exfiltrations of gas can be estimated by the constraint of the available volume v_{av}. When v_{gas} exceeds the available volume (**15,** Figure 4.1), there are exfiltrations and this amount contributes to the off gases. In the

case that v_{gas} does not occupied all the available volume, the compensation of volume is made by the air infiltrations (**16,** Figure 4.1). The mass from these estimations are updated in the storage (matrices of accumulation).

Last result. Subscripts 17 and 18, arrows

After all the process sequence, the displays of mass and energy distributions at any time of the heat can be obtained (**17,** Figure 4.1), whose units are handled in Ton and kWh respectively and the entire cycle of a step of time is over (**18**, Figure 4.1). Particularly, the global energy balance at the end of the heat is given in kWh/TLS. For the next step of time this entire sequence is repeated and so on.

It is important to mention that the temperatures are estimated simultaneously in each step of time and those influence on the energy calculations.

5.3   Simulations

A computer equipment with the descriptions detailed in chapter III was employed, the simulation of a "heat" of around 63 min to 75 min can be performed in 1.5 to 2 minutes, this means a significant advantage in comparison with other dynamic models. To prove the reliability and feasibility of the model, a base case of a 72 minutes-heat was taken to illustrate the results, whose corresponding data are displayed in Table B.2 for Fuchs® furnace. The results are analyzed and discussed below.

4.2.1   Melting of scrap

According to the operation protocols for this furnace, just a charge is regularly added per heat at around the minute 4 to 5 counting from the beginning of the process. As shown in the Figure 4.2, a charge of 59.58 Ton is added, and the evolution of the melting of scrap is displayed along with the mass increases of the steel and slag zones.
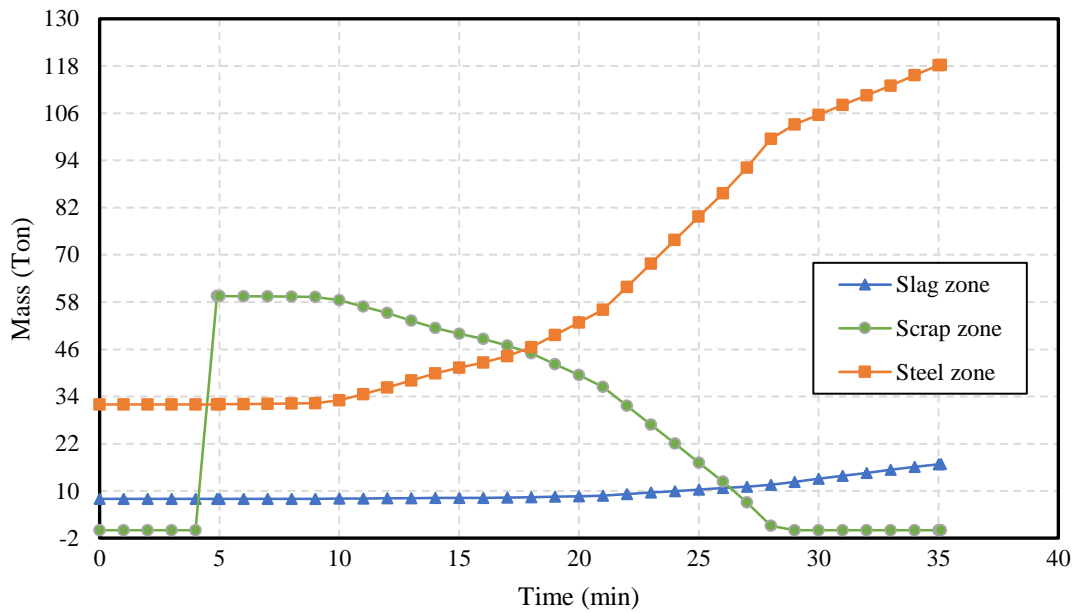
Figure 4.2 Simulation of the evolution of melting of scrap and increasing of steel and slag zone.
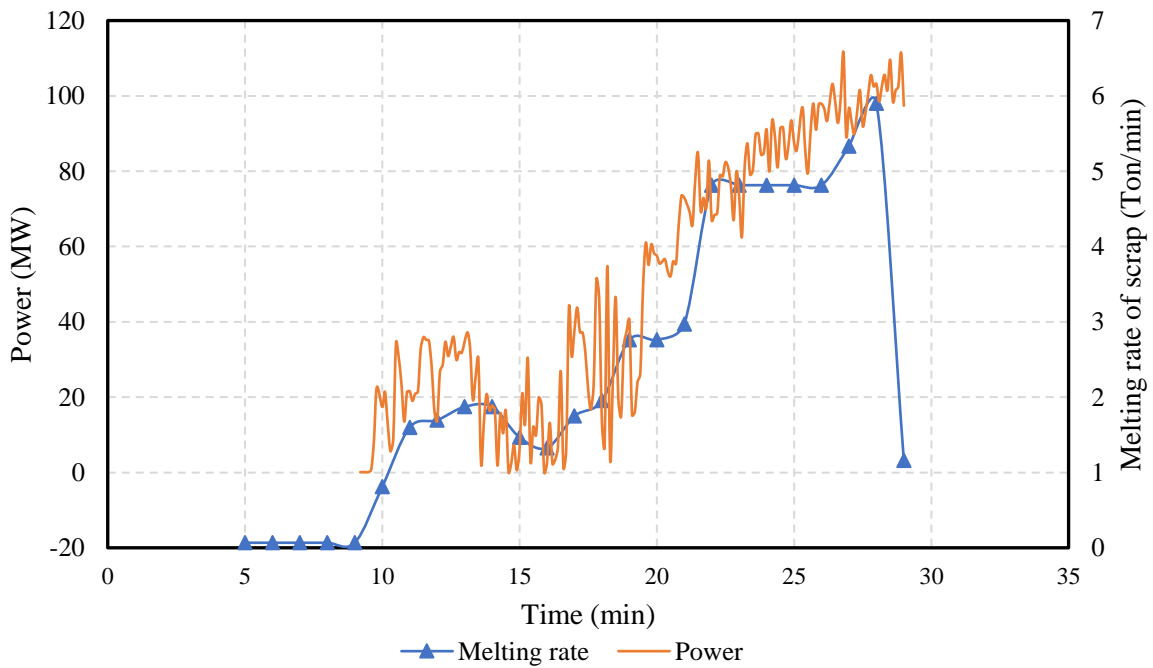

Figure 4.3 Comparison of the melting rate of scrap simulated with the power profile

According to power and material addition profiles (Figure B.1, Figure B.2 and Figure B.3) for this heat, following the good practices for the melting step, a maximum volumetric of fuel flow (average of 28 NCM/min) is supplied to heat the scrap and a moderate power flow (average 25 MW) is delivered due to the poor arc coverage at the beginning. This last condition matches with the progression of the melting rate of scrap and the power profile in the Figure 4.3, where there is a direct proportionality between them.

On the other hand, the DRI addition begins at minute 17.5 (Figure B.2), when the rise of the melting rate is noticeable (Figure 4.3) and the power is higher. Considering the instantaneous melting of DRI pellets by convection, the steel zone increases and the gangue (oxides content) is added to the slag zone simultaneously, promoting a better arc coverage, as result, the power flow can be increased at the last minutes and on.

In accordance with the observation in the steel mill for this furnace, the total time of melting occurs at 20-25 minutes after the addition of scrap, thus the simulation has a certain similarity with the real behavior.

3.2.8 Reaction velocity in the slag zone and sensitivity analysis

Since there is a remarkable interaction of the slag with the other zones and it is critical for oxides dissolution and reactions, thus, coherent results for evolution of slag compositions indicates good agreement with the transient mass balance. It should be noted that the iron oxide concentration is related to the oxidation level of the EAF and the yield, for this reason this result also gathers great significance. In general, there are 2 relationships which determine the evolution of compositions in the slag: the order of additions during the heat and the reaction velocities.

The simulation for the profile of slag compositions is shown in Figure 4.4. In certain periods some peaks are presented, this is result of material additions and reactions, for instance, at around of 21 minutes the composition of FeO reaches up to 37.64 % wt., this is due to the incipient addition of DRI (see Figure B.2) and the low volume of slag; while at the last minutes of the heat, the maximum flow of oxygen is lanced, consequently the production of FeO increases significantly, therefore, the FeO concentration is not stabilized at all at the end. The compositions of CaO and

MgO depend primarily on dolime addition, in fact they do not follow the same path as the other components, as they are fluxing agents (theoretically they do not react). From the time at which the graphite is insufflated (23 min, see Figure B.2), the decreasing of FeO is visible, because of the reduction reactions.
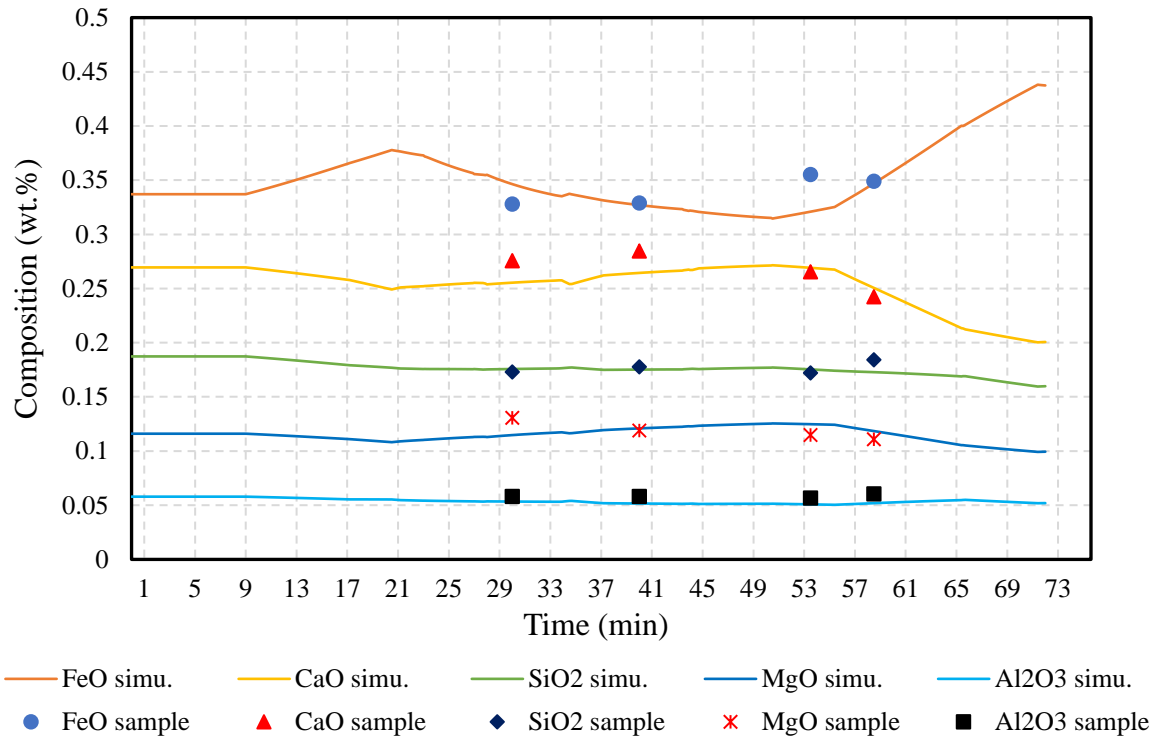

Figure 4.4 Simulation of the slag composition (wt.%) profile and comparison with samples (markers).

Also, in the Figure 4.4, a comparison between the simulation predictions (curves) and the the samples of slag (markers) is shown for the change of compositions. In order to test the quality of the simulations against the analysis of the samples, the relative errors (Er) were calculated, as shown in Table 4.1. From the perspective of the components, the main components of the slag (FeO, CaO and SiO_2) gathers smaller relative errors of $<5\%$, whereas the components in lower concentrations (MgO and Al_2O_3) have higher relative errors of $5\% \leq E_r < 11\%$. This demonstrates the relationship between the range of concentration and the relative error, then, the error increases as the general component composition is lower. The error per sample was

calculated proportionally with the mass fraction for component, where Er is on average 6%. In general, taking the results from Table 4.1, this model can simulate the behavior of the compositions in the slag with a good quality, having a mean relative error under 6%. The high E_r for MgO and Al_2O_3 are caused partly due to the lack of an oxidation mechanism for magnesium and aluminum in the steel zone for this model.

Table 4.1 Relative errors between the compositions of the simulation and the samples of slag.

	30 min	40 min	53.5 min	58.5 min	Error per component
FeO sample	0.3279	0.3288	0.3550	0.3489	
FeO simu.	0.3463	0.3270	0.3209	0.3471	4.0734%
Error	5.6229%	0.5441%	9.6036%	0.5233%	
CaO sample	0.2754	0.2846	0.2653	0.2423	
CaO simu.	0.2554	0.2644	0.2691	0.2505	4.7987%
Error	7.2704%	7.1057%	1.4297%	3.3890%	
SiO_2 sample	0.1730	0.1775	0.1720	0.1840	
SiO_2 simu.	0.1757	0.1752	0.1753	0.1728	2.7320%
%Error	1.5679%	1.3185%	1.9475%	6.0940%	
MgO sample	0.1306	0.1187	0.1146	0.1108	
MgO simu.	0.1147	0.1209	0.1248	0.1184	7.4464%
Error	12.1588%	1.8580%	8.8821%	6.8867%	
Al_2O_3 sample	0.0580	0.0579	0.0564	0.0603	
Al_2O_3 simu.	0.0534	0.0516	0.0508	0.0519	10.6786%
Error	7.9304%	10.9151%	9.9270%	13.9417%	
Error per sample	6.9101%	4.3483%	6.3580%	6.1669%	**5.9458%**

.

Even though in the last figure, the composition profiles are displayed for the 5 main components in the slag, this model also estimates the composition for C, MnO, TiO_2, CO_2 and CO, which are much lower.

To test how much the results of the kinetic model are affected by the inlet variables, a sensitivity analysis was performed for the content of CO composition in the slag zone, since it is a critical component for the slag foaming. The input variables employed were the compositions of C and FeO in hot (593.15 K) and cold (298.15 K) DRI, both were modified in a range of ±50% as shown in the Figure 4.5 and the Figure 4.6.

In the Figure 4.5 is shown the outlet variable (composition of CO) at different compositions of C in DRI (C_{DRI}) and at different times of the heat: the ending of the scrap melting, the intermediate time (50 min) and the end of the heat. At first glance the changes in the input variable does not influence significantly in the kinetics of CO.
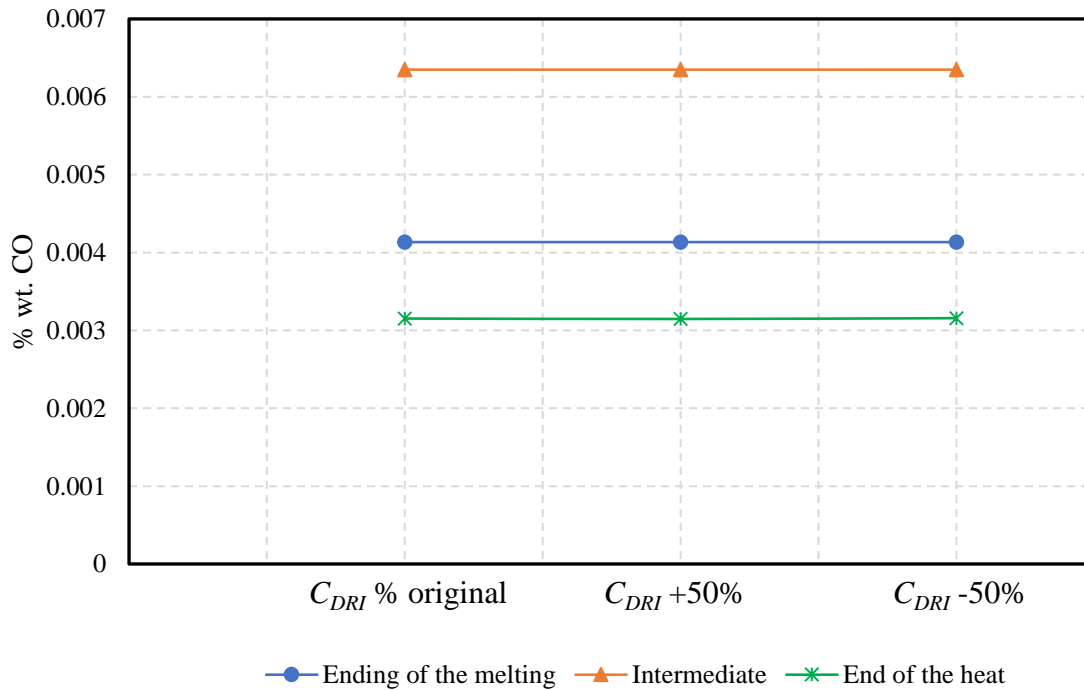
Figure 4.5 Sensitive analysis at the end of the melting, at intermediate and at the end of the heat changing the carbon content in DRI C_{DRI} .

Similarly, the concentrations of FeO in DRI were modified at the same times of the heat (Figure 4.6), where there are slight variations at the ending of the melting and at the intermediate time. However, in contrast, a noticeable sensitivity is perceived at the end of the heat on the composition of CO, having a standard deviation of 0.0008 among the values for every FeO_{DRI}.

The explanation for the obvious differences at the output variable ($CO \, wt.\%$) in both analyses may be based on the chemical interaction of the inlet variables. In this model there is just one interaction of the C_{DRI} in a reaction within the steel zone, as a result, there are less changes for the outlet variable; while, the changes in FeO_{DRI} influence is higher because it is considered that this component is added immediately to the slag zone besides it has an important interaction in 3 chemical reactions (for the kinetic model considered in this work).
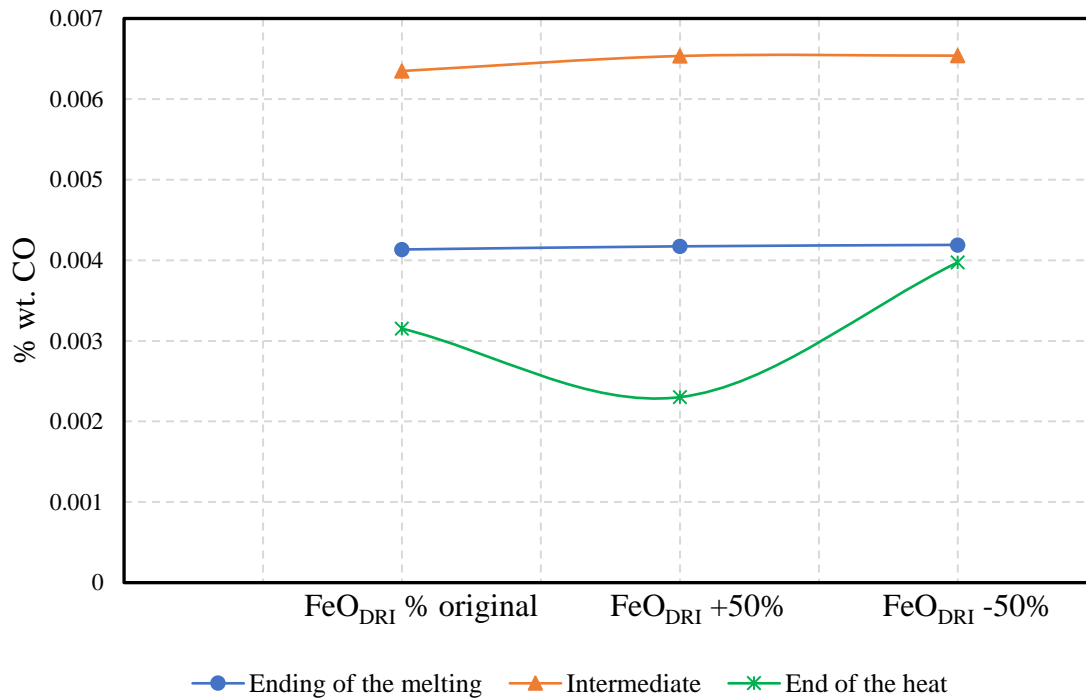

Figure 4.6 Sensitive analysis at the end of the melting, at intermediate and at the end of the heat changing the iron oxide content in DRI FeO_{DRI}.

4.2.3   Mass accumulation profile and global distribution

In the Figure 4.7, the simulation of the mass accumulation profile for each zone within the furnace (volume control) is shown. The relationship between the melting of scrap and a portion of the liquid steel accumulation was discussed previously, in this subsection the whole time of the process is discussed.

Taking as reference the Figure B.2, as DRI is added (from minute 17.5) the slag production increases, due to its level of metallization (94.39%). In general, for this heat, the production of slag is high, reaching up to 29.49 Tons, which is also related to the level of oxidation. After reaching the maximum amount of slag, a considerable decline is observed, due to the spillage of slag.

On the other hand, the gas zone has a continuous inlet (air infiltrations) and outlet (off gases), however its mass is hardly visible in the plot (Figure 4.7) due to the constant available volume inside the furnace and the high temperatures of the gases.
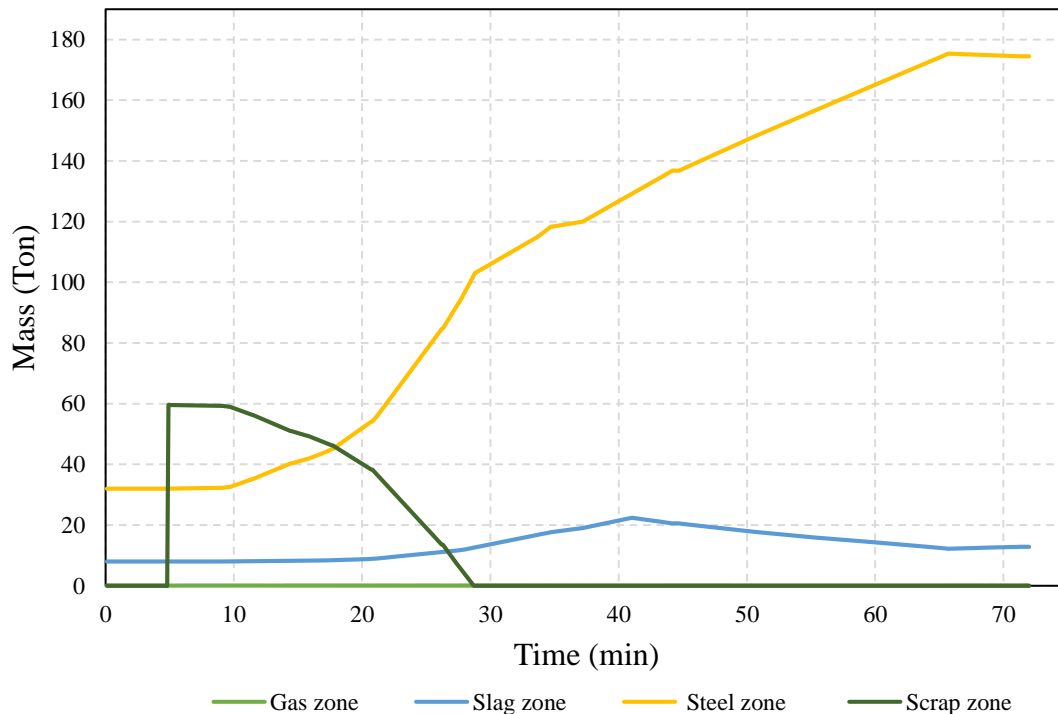
Figure 4.7 Simulation of the mass change profiles in each zone.

Regarding to the global mass balance, it is a fact that a coherent mass distribution leads to a more accurate energy distribution estimation, therefore this is one of the most important results of this work. This model estimates distribution at any time of the heat, however this simulation can be corroborated just by some data of the end of the heat as shown in the Table 4.2, where a negligible difference between inlets and outlet is observed.

Table 4.2 Global mass distribution in the Fuchs® EAF.

Inlets	Mass (Ton)	Outlets	Mass (Ton)
DRI	105.56	Stack gases	0.01
Hot heel	40.00	Hot heel	41.27
Hot load	14.39	Steel	145.45
Scrap	59.58	Slag pot	24.24
Infiltrations	63.05	Off gases	71.67
Total inlets	282.58	Total outlets	282.64

4.2.4   Temperatures estimation

The simulation of the steel-slag zone temperature profile is displayed on the following plot (Figure 4.8), in which the initial temperature for these zones, corresponds to the hot heel (1873 K). Since the first minutes of the heat neither power nor material (reactants) is added, a drop of temperature is observed just before the scrap charging, after this time (4.9 minutes), there is power supply, but the temperatures are constant due to the thermal equilibrium caused by the fusion process of the scrap, once the fusion is ended, the temperatures are constant with some peaks (occasioned by the power offs to take the samples of slag).

Near to the minute 50, the main supplies of energy (arc power and oxygen lance) for the steel zone are added at maximum flows as shown in Figure B.1 and Figure B.3, besides a greater arc coverage is reached having a maximum convection from the arc to the bath, as a consequence a greater increase of the temperature is noticed from that time until the end, reaching a maximum of 1909 K.
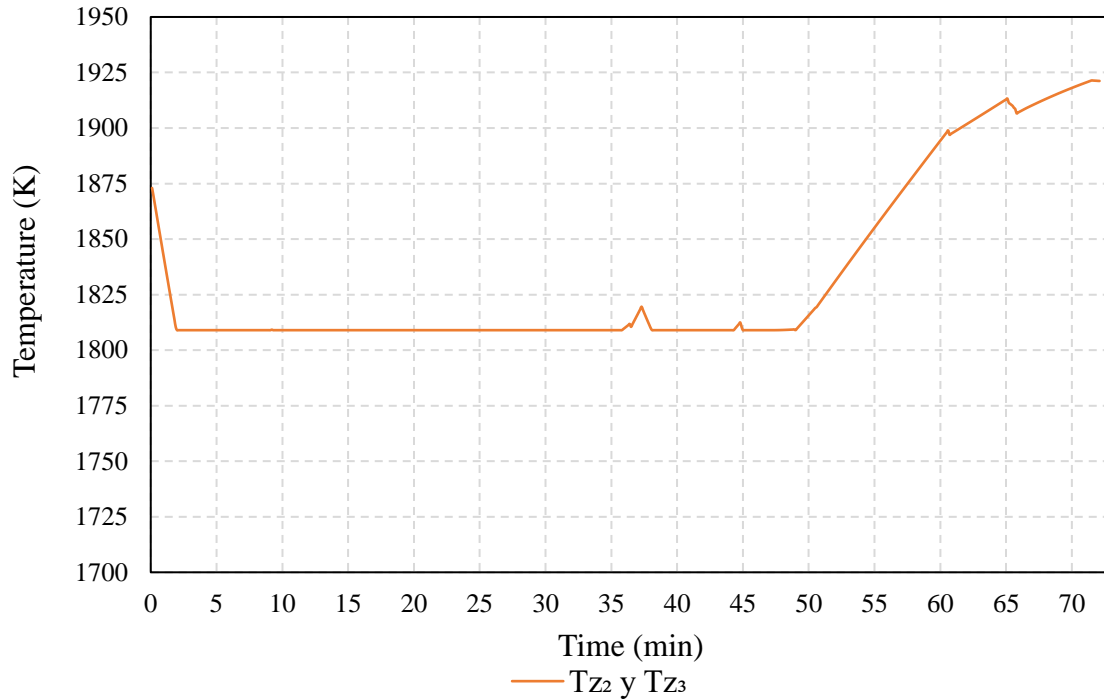
Figure 4.8 Simulation of the steel-slag zones temperature profile

.

Making a comparison with the real bath temperature measures taken at the minute 50 of 1809 K and at the minute 66 of 1907 K, the simulation leads to a good estimation of 1815 K and 1907.25 K respectively.

On the other hand, the simulation of the gas zone temperature profile is shown in Figure 4.9, where the initial temperature is set at 400 K, but since there are continuous gas extraction and air infiltrations besides the lack of energy sources, the temperature drops until 300 K before the scrap charging.

After the charging, a significant increase is noticed, due to the incipient addition of power from the arc and natural gas (in fact, the maximum flow for preheating), afterwards the gas temperature shows a more stable behavior due to the thermic equilibrium of the fusion of the scrap. After this process, the temperatures increase at higher rates due to the rising of the production of CO and CO_2 in the steel and slag zones and the bubble time of residence in the slag.
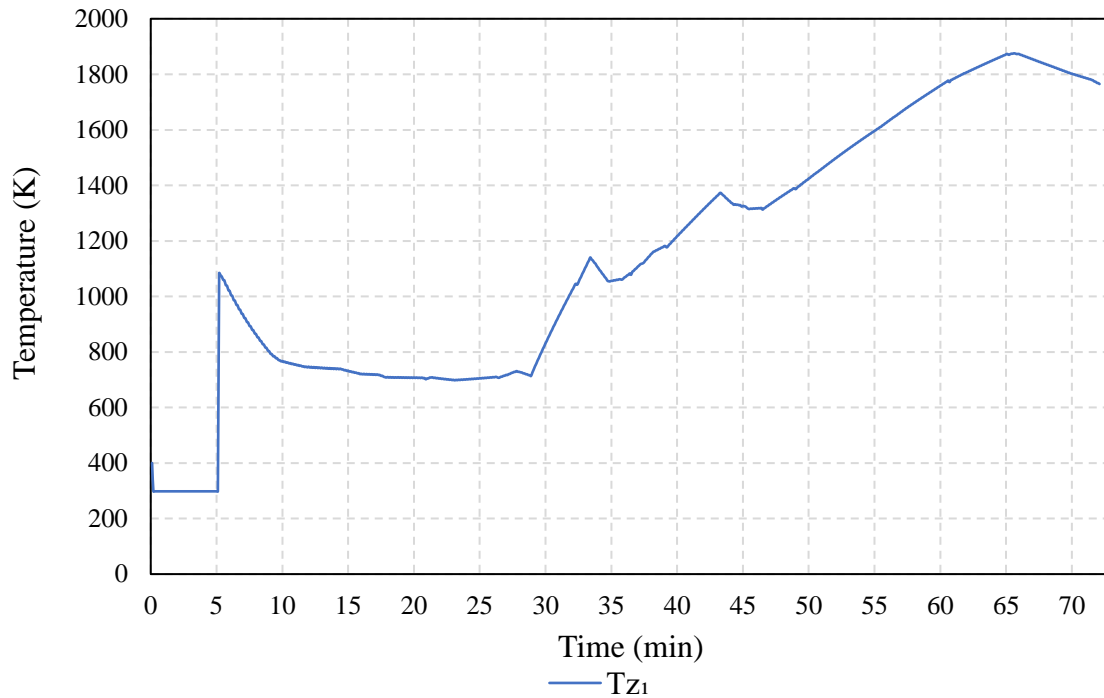
Figure 4.9 Simulation of the gas zone temperature profile.

It should be noted hat the gas composition is also related to the heat absorbed (particularly by the off gases), as can be observed in Table 4.3, the critical components with the higher heat capacity are the water, CO and CO_2, thus, along with the air, cause a significant outlet of energy.

Comparing the generation of CO and CO_2, the equilibrium of CO_2 is preferential for the gas mixture below 1600 K, while over this temperature CO is favored (Smith, J. M., 1996). Since 75% of the heat approximately is below 1600K, the CO_2 production is higher in the global off gases composition.

Table 4.3 Global off gases composition.

Gas component	CH_4	H_2O	H_2	N_2	C_9H_{20}	CO	CO_2	O_2
Composition wt.%	-	0.0284	-	0.6346	0.0047	0.0947	0.1441	0.1303

4.2.6 Energy accumulation profile and global distribution

The outlet energy distributions can be estimated at any time of the heat cumulatively, as shown in the following profiles (Figure 4.10), where the highest energy corresponds to the liquid steel. At the beginning of the heat the energy of the steel zone increases slightly (low power from the arc), however around the time of the fusion (minute 28) the highest heat rate occurs due to the heat of phase transformation and the meaningful increase of power from the arc. Until this point the bath temperature and energy accumulation of steel zone can be raised, even the heat rate is maintained steady with the injection of O_2 until the flat bath temperature is reached.

The off gases are the second highest outlet of energy. Since there is a thermal equilibrium among the steel, the slag and the gas zone during the fusion, the increasing of the energy occurs slowly, also around the end of the fusion, there is a rise in the heat rate. Then, the increasing is almost linear until the power is off at the minute 66.
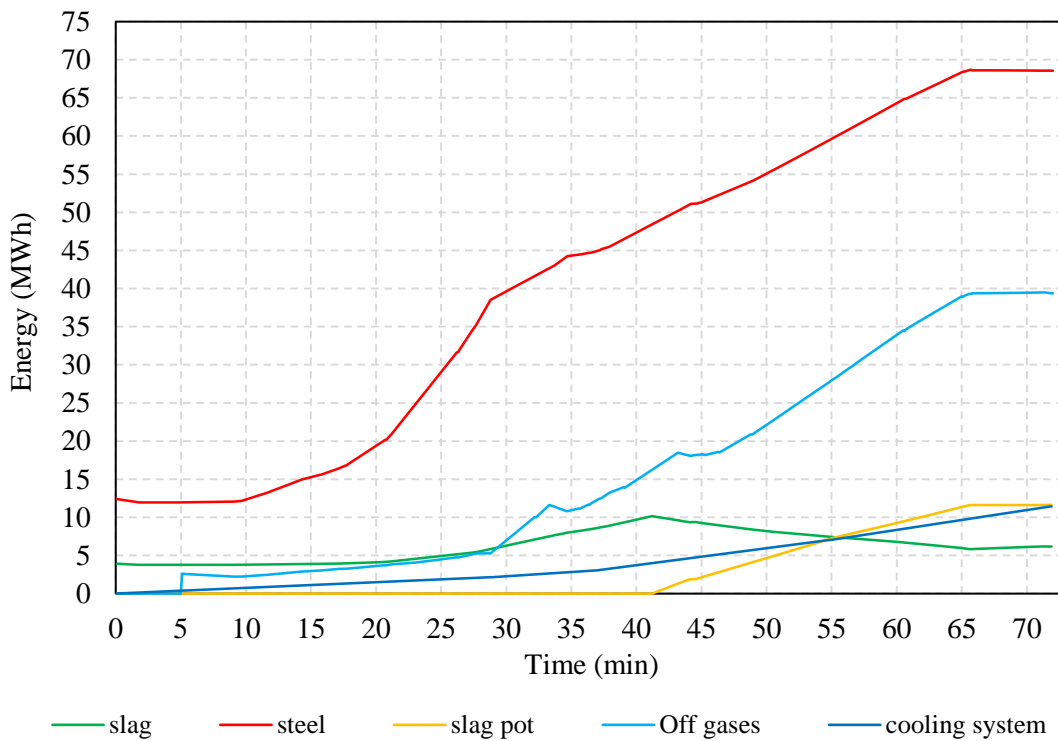

Figure 4.10 Simulation of the energy distribution profiles (MWh).

Regarding the rest of the energy outlets, the slag zone energy accumulation drops when the spillage occurs, thus, the slag pot accumulation increases. The cooling system outlet increases meaningfully once all the scrap is molten and as the bath temperature can be raised reaching $\Delta T_{max} = 7\ K$ in the panels. The energy of the stack gases is almost negligible due to the continuous infiltrations (cooling) and outlets in this zone; the same occurs for the losses, which is practically the residual result from the energy distributions at any step of time.

The global energy distribution for the final stage of the heat is shown in the Figure 4.11, where the inlets (left side) and outlets (right side) of energy are displayed. The total energy inlet is about 943 kWh/TLS for an amount of 145.45 TLS, in which the main source is the electrical energy (497 kWh/TLS), followed by the carbon combustion (133 kWh/TLS), the natural gas combustion (80
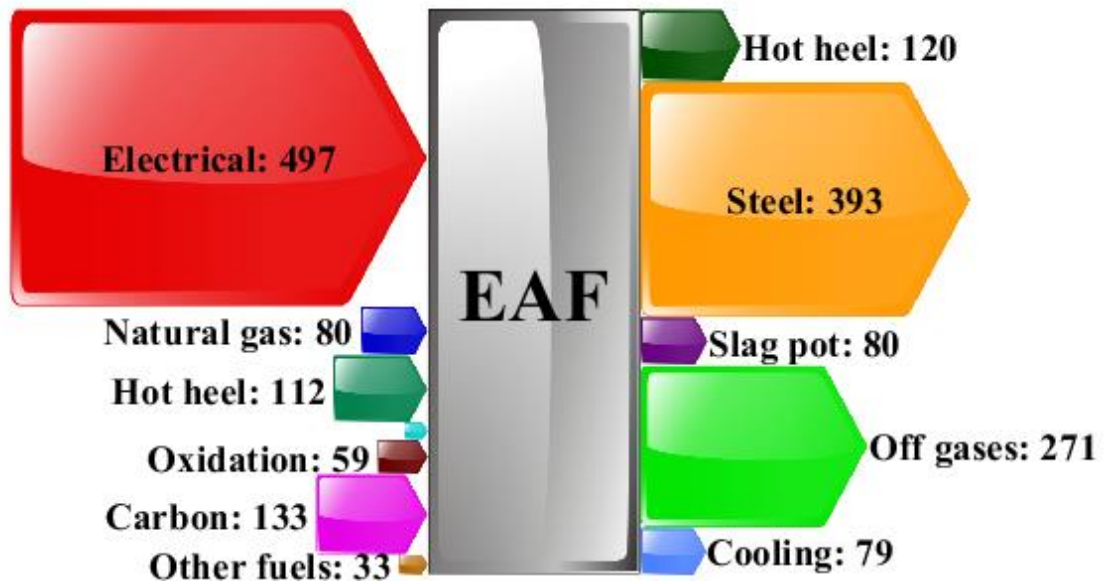

Figure 4.11 Global energy distribution kWh/TLS (at the time of the tapping).

kWh/TLS), and the oxidation (59 kWh/TLS). For this case, there is a moderate energy from the carbon combustion due to the lack of anthracite addition, this also contributes to slow down the reduction reactions, as a result the oxidation energy level is high. It is noted that under these conditions a proper flat bath temperature can be reached and maintained, this goes together with

the reduction of the Tap-to Tap-time, conversely, the yield of iron is slightly sacrificed, since a certain amount that is leaving in the slag could not be recovered via reduction.

It is a fact that the largest energy output is the inherent energy in the steel (393 kWh/TLS), followed by the energy lost in the off gases (271 kWh/TLS), the slag pot (80 kWh/TLS) and the cooling system (79 kWh). Just the theorical sinks of energy (off gases and cooling system) represent about 37% of the total inlet energy. According to the general criteria, the net efficiency for this equipment is about 51%, that compared with conventional EAF efficiencies from 50% to 60% (Pfeifer, Kirschen and Simoes, 2005) is in the range.

Chapter V

Conclusions

5.2 Summary of conclusions

First, it has been demonstrated that it is possible to build a flexible MEB model with transient approach based on some phenomena that occurs inside the EAF. It was able to estimate the mass and energy distribution at any time of the heat and some unknown variables such as air infiltrations and off gases, despite some unavailable data. With the display of these calculations, the behavior inside the electric arc furnace can be predicted with a certain accuracy, and preliminar decisions about the protocol improvements can be made. It should be noted that the employment of some adjustment parameters was required due to the complex nature of this process and the unavailable data.

Despite of the simple formulation of the module of the melting of scrap, the simulation was closed to the real behavior, having a result of 23 minutes of fusion, which is within the range for this furnace, but this may be subject to slight variations due to the random size and shape of the scrap. Also, it was noted that the simulation of the fusion was apparently synchronized with some addition times related to the steel zone, such as DRI and power from the arc. The advantage of having this estimation was to know the actual status of the steel zone at any moment and the portion of it which interacts with the other zones.

The simulation of the evolution of slag zone composition demonstrated to have a direct relationship with the additions of DRI, O_2 lance-graphite and dolime, which contribute, react and work as fluxing agents respectively, this overview is useful to make decisions to maintain a balance

between the oxidation and the reduction, this impacts on the production and the costs. Also, a good estimation was observed for the behavior of the compositions, having an overall relative error of less than 6% in comparison with the 4 samples of slag. These E_r are lower (<5%) for the main components: FeO, CaO and SiO_2; whereas for the components in a lower proportion showed higher E_r (5%-11%) due to the lack of oxidation mechanisms for Mg and Al in this model. In general, these results are indicators of a good agreement with the mass and energy calculations.

On the other hand, the sensitive analysis for the composition of CO in the slag zone by varying C and FeO content in DRI (input variables), only presented a noticeable sensitivity with the change of FeO just at the end of the heat, while in the rest of the cases no significant CO variations were observed. The difference between these analyses may be based on the chemical interaction of the input variables according to the proposed mechanisms, in this case FeO has more, thus the sensitivity tends to be higher.

Regarding the temperature profiles estimations, in general there is a coherence between the additions of energy and the stages of the heat, for instance, during the fusion process the slag-steel temperature and the gas temperature are maintained in thermal equilibrium. For gas zone one of the most important variables is the composition, as it is related with the heat absorbed (for different heat capacities), in turn the temperature is an indicator of the tendency of conversion, in this case from CO to CO_2.

The most relevant results from this work were the general overviews of the distribution and accumulation profiles of mass and energy at any time of the heat. Although the corroboration of the mass distribution estimation was performed with data from the end of the heat, a good result was obtained with negligible differences.

The calculation of the energy distribution and the profiles go together with the mass distribution for each zone, the estimation of unknown mass flows, the electric energy and the chemical reactions. As it is well known the main sources of energy are the electric and the carbon energy, while the main losses are presented by the heat absorbed in the off gases and the cooling system. To validate the energy balance in each step of time, the variable "other losses" was employed to quantify the differences between energy inputs and outputs. It should be noted that the efficiency of this EAF is in the typical range for a conventional furnace.

These estimations for mass and energy distributions are useful to improve the time and amount of additions and to maintain a balance between the steel production and energy consumption, this can be performed by the operation protocols, as a result, costs savings may be obtained. Since the main sink of energy corresponds to the off gases, it represents an opportunity to improve much more the furnace efficiency, this can be achieved by improving the slag foaming to maintain the arc coverage or by the heat recovering with the preheating of metallic charge; while the cooling system losses may be decreased more by the increase of the slag layer thickness in the panels.

5.2 Contributions

A comprehensive transient approach for the mass and energy balance in the EAF was developed for predictive purpose. It was based on the inherent phenomena in the process of a heat and goes together with the estimation of mass and energy flows.

The kinetics model can predict the behavior of the composition of slag at any time, it employed a proposed mechanism which is underpinned by the literature reviewed. This model also could be useful for furnaces that does not have instrumentation equipment to measure gas variables since this enables an estimation of infiltrations and off gases, gas compositions and temperatures.

And last, this model provides overviews of mass and energy distribution and information of chemical and operation parameters at any time of the heat, due to the flexibility of the model structure it may be considered as a basis of a dynamic optimization model to improve the operation protocols and energy savings. Besides, it is possible to adapt a heat transfer model, which could provide information about dynamic simulation of slag foaming, with this tool it is possible to obtain a better arc coverage, and as result, to increase the energy savings in the off gases and the harnessing in the liquid bath, this could enhance the efficiency of the EAF much more.

5.3   Recommendations and future work

In order to improve this model, the following work for complementing is recommended:

- To consider more species for the entire model, even their low contents, this may improve the accuracy of the model.

- To include more oxidation reactions within the proposed mechanism of the steel and slag, particularly for Mg, Al, and alloys (just in case of considering more species).

- To carry out a more rigorous study with more slag samples at smaller time intervals and with more types of heat, with this information readjustments of the rate constants can be made for the accuracy enhancing.

- To elaborate a more detailed analysis in the heat transfer of the scrap fusion and to employ especial factors which consider the shape and the size of the scrap.

- To develop a dynamic heat transfer model and to assemble it to this model. This model could consider the 3 forms of delivered energy from the arc: electrons, convection and radiation, for the last one, to build a circuit based in Kirchhoff law. With this complement, some slag foaming simulations could be performed in order to watch the best scenarios for arc coverage; besides, it could also predict the unrecognized losses and the accurate cooling system and off gases losses.

- Once assembled the heat transfer model, to make a balance in the cooling panels, slag layer and gases, so that it could estimate better approximations for gas temperature.

- To simulate several scenarios with different types of heat and to corroborate with operation data, this enables the overview for the best operation conditions.

- With the proper factors of adjustments and the integration of the heat transfer model this work could be used as guideline of an optimization model.

Appendices

Appendix A. Slag viscosity correlations

a) Riboud model

The accumulative molar fractions X' are defined by the following equations:

$$X'_{SiO_2} = X_{SiO_2} + X_{P_2O_5} + X_{TiO_2} + X_{ZrO_2} \qquad \text{A-1}$$

$$X'_{Al_2O_3} = X_{Al_2O_3} + \{X_{P_2O_5}\} \qquad \text{A-2}$$

$$X'_{CaO} = X_{CaO} + X_{MgO} + X_{FeO} + X_{Fe_2O_3} \\ + \{X_{MgO} + X_{NiO} + X_{CrO} + X_{ZnO} + X\_Cr_2O_3\} \qquad \text{A-3}$$

$$X'_{Na_2O} = X_{Na_2O} + X_{K_2O} + \{X_{Li_2O}\} \qquad \text{A-4}$$

Having defined the molar fractions, the viscosity is expressed as a function of temperature:

$$\mu = A \cdot T \cdot \exp{\frac{B}{T}} \qquad \text{A-5}$$

Where A and B are parameters in function of cumulative molar fractions:

$$A = \exp(-19.81 + 1.73X'_{CaO} + 5.82X'_{CaF_2} + 7.02X'_{Na_2O} - 35.76X'_{Al_2O_3} \qquad \text{A-6}$$

$$B = 31140 - 23896X'_{CaO} + 46356X'_{CaF_2} - 39159X'_{Na_2O} + 68833X'_{Al_2O_3} \qquad \text{A-7}$$

b) Urbain model

The molar fraction is classified three categories:

→ Glass formers:

$$X_G = X_{SiO_2}$$

A-8

→ Network modifiers:

$$X_M = X_{CaO} + X_{MgO} + X_{CaF_2} + X_{FeO} + X_{MnO} + X_{CrO} + X_{NiO} + X_{K_2O}$$
$$+ 2X_{TiO_2} + X_{ZrO_2}$$

A-9

→ Amphoteric compounds:

$$X_A = X_{Al_2O_3} + X_{B_2O_3} + X_{Fe_2O_3} + X\_Cr_2O_3$$

A-10

Where slag viscosity is estimated by the Weymann expression:

$$\mu = A \cdot T \cdot \exp^{\frac{1000B}{T}}$$

A-11

Parameters *A* and *B* are calculated by the following Equations:

$$\ln A = -(0.29B + 11.57)$$

A-12

$$B = B_0 + B_1 X_{SiO_2} + B_2 X_{SiO_2}^2 + B_3 X_{SiO_2}^3$$

A-13

B_0, $B1$, $B2$ and $B3$ are parameters obtained by Equation the following equations:

A-14

$$\alpha = \frac{X_M}{X_M + X_A}$$

A-15

$$B_0 = 13.8 + 39.9355\alpha - 44.049\alpha^2$$

$$B_1 = 30.481 - 117.1505\alpha + 139.997\alpha^2 \qquad \text{A-16}$$

$$B_2 = -40.9429 + 234.0486\alpha - 300.04\alpha^2 \qquad \text{A-17}$$

$$B_3 = 60.7619 - 153.9276\alpha + 211.1616\alpha^2 \qquad \text{A-18}$$

Appendix B. Operational data

B.1 Operation data

Table B.1 Check list for data request.

Time of data collection	Data	Done?
Before the heat	Analysis of DRI.	☐
	Analysis of dolime.	☐
	Analysis of anthracite	☐
Start of the heat	Mass of hot heel (TON).	☐
	Analysis of slag in hot heel (final analysis of the previous heat).	☐
	Temperature of hot heel.	☐
During the heat	Mass and energy flow profiles (HARSCO).	☐
	Mass of scrap (TON).	☐
	Analysis of slag at different times (just for kinetic testing)	☐
End of the heat	Mean temperature of flat bath.	☐
	Total material consumption	☐
	Spilled slag mass (TON)	☐

Table B.2 Parameters used to estimate the mass and energy balances of the EAF Fuchs

Material additions (Ton)		Volume additions (NCM)	
Hot heel steel	36.0000	Oxygen lance	3542.0000
Hot heel slag	9.0000	Oxygen burners	1632.0000
Scrap	59.5800	Natural gas	1023.0000
Cold DRI	73.4860	**Mass outlets defined (Ton)**	
Hot DRI	32.2030	Tapped steel	145.4500
Dolime	9.8150	**Operational times (min)**	
Graphite	0.5450	Tap-to-tap time	72
Carbon in the basket	0.0000	Power on time	56
Anthracite	0.0000	**Energy additions (MWh)**	
Temperature of additions (K)		Electric energy	72.6000
Cold DRI	300.15	Fuel	11.6360
Hot DRI	593.15	**Cooling water flows (m^3/h)**	
Dolime	298.15	Sidewalls	900
Graphite	298.15	Roof	500
Scrap	298.15	Elbow	200
Oxygen lance/burners	298.15	Electrode	3
Natural gas	298.15	**Temperature of cooling system (K)**	
Infiltrations	298.15	Initial temperature panels	308.15
Temperature of bath (K)		Increment in cooling water	6
Initial	1873	Water cooling electrode	298.15
Final	1907		

Table B.3 Estimated parameters in the EAF Fuchs.

Mass inlets (Ton)		Mass outlets (Ton)	
Infiltrations	63.0498	Slag pot	24.2422
Energy contributions (MWh)		Off gases	71.6715
Carbon	19.3850	Hot heel	41.2782

Oxidation	8.5860	Final zone temperature (K)	
Other fuels	4.872	**Steel zone**	1913
		Slag zone	1913
		Gas zone	1465

Table B.4 Chemical composition (Wt.%) for hot heel slag.

Hot heel slag	FeO	SiO_2	Al_2O_3	CaO	MgO	MnO	TiO_2
	0.3370	0.1873	0.0579	0.2695	0.1160	0.0196	0.0127

Table B. 5 Chemical composition (Wt.%) for material additions.

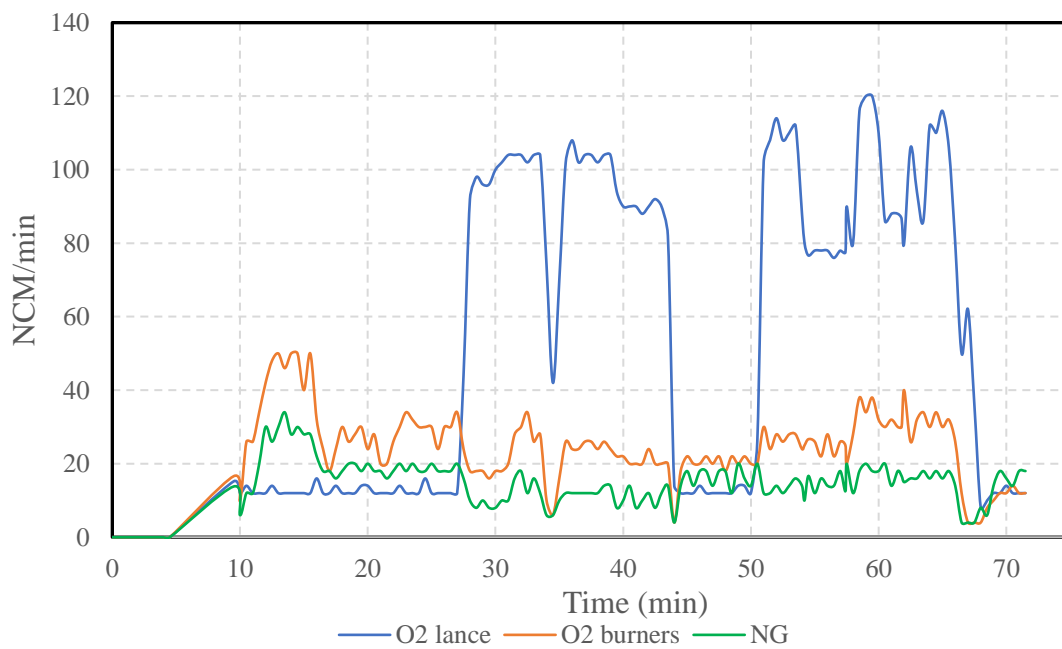| Material	C	Fe	FeO	Fe_2O_3	SiO_2	Al_2O_3	CaO	MgO
Cold DRI	0.0368	0.8201	0.0511	0.0140	0.0329	0.0136	0.0185	0.0130
Hot DRI	0.0368	0.8210	0.0464	0.0178	0.0329	0.0136	0.0185	0.0130
Dolime	-	-	-	-	0.1600	-	0.6000	0.2400

B.2 Addition profiles
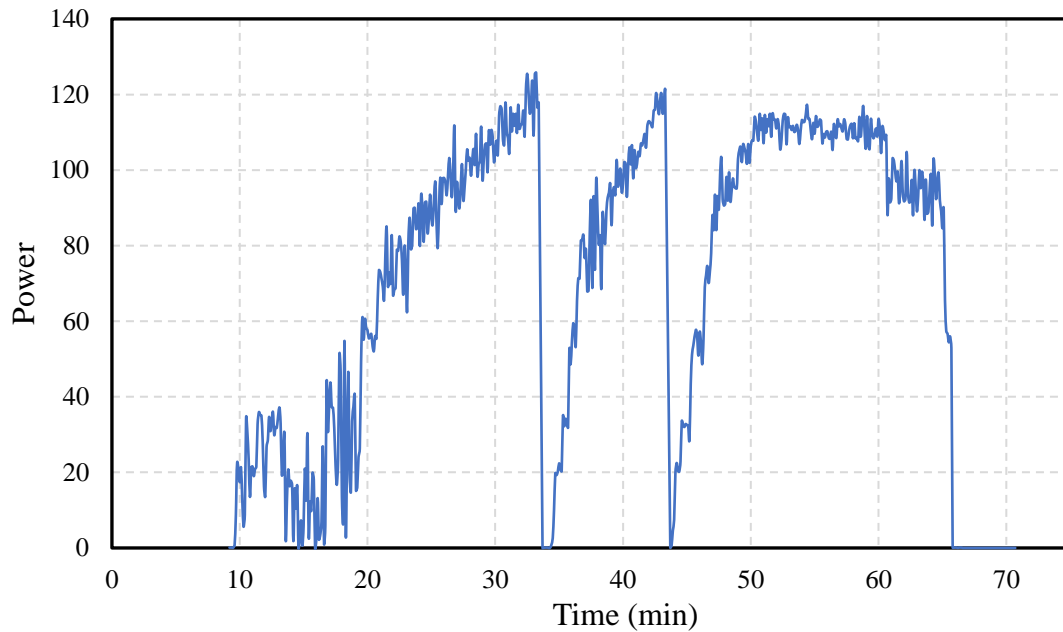
Figure B.1 Profile of power addition.
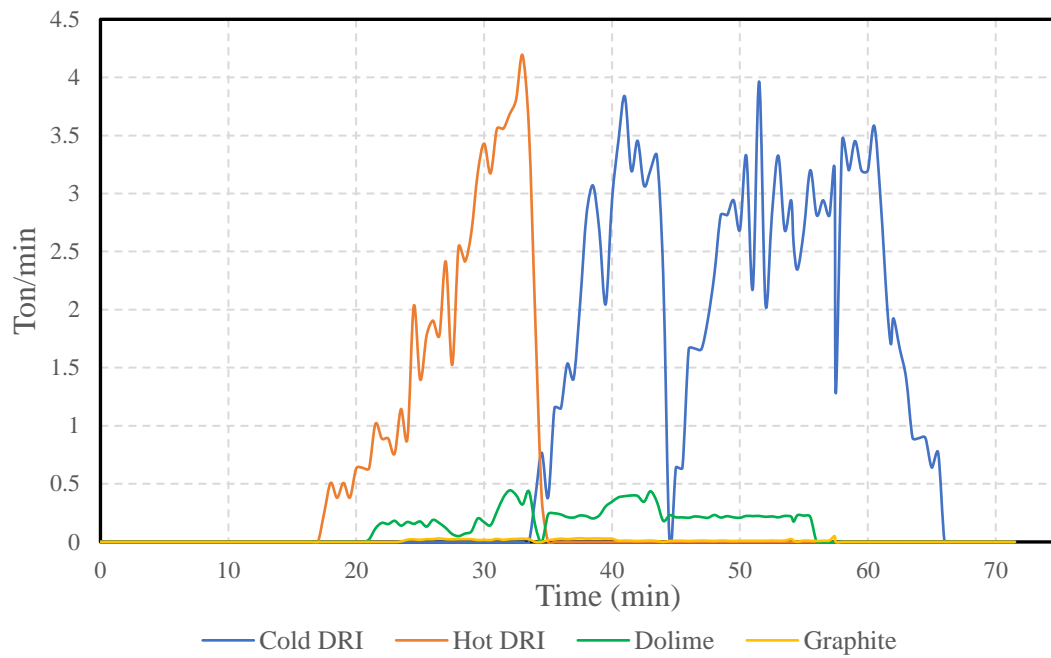
Figure B.2 Profiles of material additions, mass flows.

Figure B.3 Profiles of gases additions, volumetric flows.

Appendix C. Useful properties for the energy balance

Table C. 1 Enthalpies of formation at 298.15K.

Specie	$\Delta H°_f \left(\frac{KJ}{mole}\right)$	Specie	$\Delta H°_f \left(\frac{KJ}{mole}\right)$
O_2	0	MnO	-385.18
CH_4	-74.84	C	0
CO_g	-110.53	Al	0
CO_2	-393.51	Al_2O_3	-1675.7
H_2O_l	-285.83	Fe_2O_3	-824.2
H_2	0	CaO	-635.09
N_2	0	MgO	-601.5
C_9H_{20}	-275.7	Mn	0
Fe	0	P	0
FeO	-266.3	TiO_2	-945
SiO_2	-851	Si	0

Table C. 2 Standard Gibbs free energy for gas zone species.

	Standard Gibbs free energy $\Delta G°_f \left(\frac{KJ}{mole}\right)$
CH_4	-50.8356
H_2O	-228.5887
H_2	0
N_2	0
C_9H_{20}	-121.877
CO	-137.27704
CO_2	-394.38384
O_2	0

- Specific heat capacity is given by Equation   and its units are $\frac{J}{mole \cdot K}$.

$$cp = a + b \cdot T + c \cdot T^{-2} + d \cdot T^2$$

Table C.3 Specific heat capacities and transition enthalpies **recovered from (Trejo, 2012).**

Specie	a	b × 10³	c × 10⁻⁵	d × 10⁶	Range of T	T of transition	$\Delta \widehat{H}$ of transition
O_2	29.977	4.187	-1.675	-	-	-	-
CH_4	12.456	76.740	1.449	-18.016	298-2500	-	-
CO	28.95	4.103	-0.461	-	298-2500	-	-
CO	44.171	9.043	-8.541	-	298-2500	-	-
C	11.183	0.01095	489,110	-	-	-	-
H_2O (l)	75.312	-	-	-	298-373	373	40,743
H_2O (g)	30.019	10.718	0.335	-	298-2500	-	-
H_2	27.298	3.266	0.502	-	298-3000	-	-
N_2	27.884	4.271	-	-	298-2500	-	-
C_9H_{20}(l)	284.577	-	-	-	298-424	424	37,806
C_9H_{20}(g)	102.953	548.019	-30.388	-164.056	424-1500	-	-
FeO(s)	50.836	8.621	-3.312	-	298-1650	1650	24,074
FeO(l)	68.245	-	-	-	-	-	-
Si(s)	22.839	3.860	-3.542	-	298-1685	1685	50,241.6
Si(l)	27.214	-	-	-	1685-	-	-
MnO(s)	46.515	8.122	-3.684	-	298-1800	1800	54,428.4
MnO(l)	60.709	-	-	-	1800-3000	-	-
Al(s)	31.397	-16.404	-3.609	20.767	298-933	933	10,718
Al(l)	31.769	-	-	-	933-2767	-	-
CaO	49.655	4.522	-6.950	-	298-2888	-	-
MgO	49.015	3.144	-11.447	-	298-3098	-	-

Specie	a	b × 10³	c × 10⁻⁵	d × 10⁶	Range of T	T of transition	ΔĤ of transition
$FeO_{(s\alpha)}$	17.49	24.769	-	-	298-1033	1033	5,105
$FeO_{(s\beta)}$	37.66	-	-	-	1033-1187	1187	670
$FeO_{(s\gamma)}$	7.7	19.5	-	-	1187-1665	1665	837
$FeO_{(s\delta)}$	28.284	7.53	-	-	1665-1809	1809	13,807
$FeO_{(l)}$	35.4	3.74	-	-	1809-	-	
$SiO_{2(s\alpha)}$	46.930	31.522	-10.099	-	298-543	543	1,343.9
$SiO_{2(s\beta)}$	71.674	1.892	-39.084	-	543-1996	1996	9,587
$SiO_{2(l)}$	85.829	-	-	-	1996-3000	-	-
$Mn_{(s\alpha)}$	20.758	18.740	-	-	298-600	600	-
$Mn_{(s\beta)}$	24.024	13.469	-	-	600-980	980	2,227.37
$Mn_{(s\gamma)}$	33.457	4.250	-	-	980-1360	1360	2,122.708
$Mn_{(s\delta)}$	31.736	8.374	-	-	1360-1410	1410	1,879.873
$Mn_{(s\varepsilon)}$	33.603	8.269	-	-	1410-1517	1517	12,066.35
$Mn_{(l)}$	46.055	-	-	-	1517-2335	2335	226,221.17
$Mn_{(g)}$	20.967	-	-	-	2335-2600	-	-
$Al_2O_{3(s\alpha)}$	103.921	26.285	-29.111	-	298-800	800	118,486
$Al_2O_{3(s\beta)}$	120.597	9.198	-48.399	-	800-2327	-	-
$Fe_2O_{3(s\alpha)}$	98.348	77.874	-14.863	-	298-953	953	669.88
$Fe_2O_{3(s\beta)}$	150	-	-	-	953-1053	1053	-
$Fe_2O_{3(s\gamma)}$	132.763	7.369	-	-	1053-1730	-	-
$TiO_{2(s\alpha)}$	44.254	15.072	-7.787	-	298-1264	1264	23,475.044
$TiO_{2(s\beta)}$	56.518	8.332	-	-	1264-2023	2023	54,428.4
$TiO_{2(l)}$	54.428	-	-	-	2023-3934	-	-

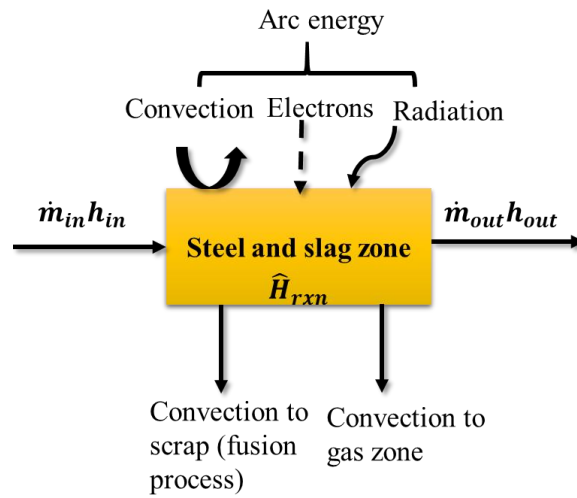## Appendix D. Energy balance schemes for each zone

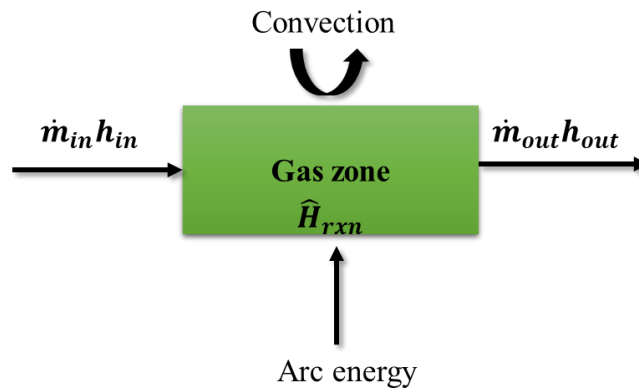*Figure D.1 Scheme of the energy balance for steel-slag zone.*

Figure D.2 Scheme of the energy balance for the gas zone.

References

Alacero (2018) *América Latina: Importaciones de acero y precio promedio*. Available at: https://www.alacero.org/es/page/prensa/noticias/america-latina-importaciones-de-acero-y-precio-promedio-desde-china-disminuyen.

Association, W. S. (2016) 'Energy use in steel industry', p. 3.

Association, W. S. (2017) *World steel in figures 2017*, p.17.

Association, W. S. (2018) 'Fact sheet: Energy use in the steel industry.' World steel association. Bekker, J. G., Craig, I. K. and Pistorius, P. C. (1999) 'Modeling and Simulation of an Electric Arc Furnace Process', *ISIJ International*, 39(1), pp. 23–32. doi: 10.2355/isijinternational.39.23.

Bekker, J. G., Craig, I. K. and Pistorius, P. C. (2000) 'Model predictive control of an electric arc furnace off-gas process', *Control Engineering Practice*, 8(4), pp. 445–455. doi: https://doi.org/10.1016/S0967-0661(99)00163-X.

Bikerman, J. J. (1938) 'The unit of foaminess', *Trans. Faraday Soc.* The Royal Society of Chemistry, 34(0), pp. 634–638. doi: 10.1039/TF9383400634.

Bisio, G., Rubatto, G. and Martini, R. (2000) 'Heat transfer, energy saving and pollution control in UHP electric-arc furnaces', *Energy*, 25(11), pp. 1047–1066. doi: http://dx.doi.org/10.1016/S0360-5442(00)00037-2.

Çamdali, Ü. and Tunç, M. (2003) 'Exergy analysis and efficiency in an industrial AC electric ARC furnace', *Applied Thermal Engineering*. Pergamon, 23(17), pp. 2255–2267. doi: 10.1016/S1359-4311(03)00192-3.

Çamdalı, Ü. and Tunç, M. (2002) 'Modelling of electric energy consumption in the AC electric arc furnace', *International Journal of Energy Research*. John Wiley & Sons, Ltd., 26(10), pp. 935–947. doi: 10.1002/er.829.

Canacero (2018) *Canacero*, *Panorama siderúrgico 2018*. Available at: http://www.canacero.org.mx/Es/assets/infografia_canacero_2018.pdf.

Crucible industries (2016) *Pioneering research and technology*. Available at: https://www.crucible.com/history.aspx?c=20.

Ghag, S. S., Hayes, P. C. and Lee, H.-G. (1998) 'Physical Model Studies on Slag Foaming', *ISIJ International*, 38(11), pp. 1201–1207. doi: 10.2355/isijinternational.38.1201.

Hesketh, R. P., Etchells, A. W. and Russell, T. W. F. (1991) 'Bubble breakage in pipeline flow', *Chemical Engineering Science*, 46(1), pp. 1–9. doi: https://doi.org/10.1016/0009-2509(91)80110-K.

IEA (2017) *World energy balances: overview*.

Ito, K. and Fruehan, R. J. (1989) 'Study on the foaming of CaO-SiO2-FeO slags: Part I. Foaming parameters and experimental results', *Metallurgical Transactions B*, 20(4), pp. 509–514. doi: 10.1007/BF02654600.

J. L. G. Sánchez, M. A. R.-A. and A. N. C. (2009) 'Power delivery from the arc in AC electric arc furnaces with different gas atmospheres', *Steel Research International*, 80(2), pp. 113–120.

Jiang, R. and Fruehan, R. J. (1991) 'Slag foaming in bath smelting', *Metallurgical Transactions B*, 22(4), pp. 481–489. doi: 10.1007/BF02654286.

Kirschen, M., Badr, K. and Pfeifer, H. (2011) 'Influence of direct reduced iron on the energy balance of the electric arc furnace in steel industry', *Energy*, 36(10), pp. 6146–6155. doi: http://dx.doi.org/10.1016/j.energy.2011.07.050.

Kirschen, M., Velikorodov, V. and Pfeifer, H. (2006) 'Mathematical modelling of heat transfer in dedusting plants and comparison to off-gas measurements at electric arc furnaces', *Energy*, 31(14), pp. 2926–2939. doi: https://doi.org/10.1016/j.energy.2005.12.006.

Li, Y. and Fruehan, R. J. (2003) 'Computational fluid-dynamics simulation of postcombustion in

the electric-arc furnace', *Metallurgical and Materials Transactions B*, 34(3), pp. 333–343. doi: 10.1007/s11663-003-0079-9.

Madias, J. (2013) 'Electric arc furnace steelmaking', in *Ironmaking and steelmaking*, pp. 271–299. Matsuura, H. and ard J. Fruehan, R. (2009) 'Slag Foaming in an Electric Arc Furnace', *ISIJ International*, 49(10), pp. 1530–1535. doi: 10.2355/isijinternational.49.1530.

Midrex technologies, I. (2014) 'The MIDREX porcess', p. 12.

Mills, K. C. and Keene, B. J. (1987) 'Physical properties of BOS slags', *International Materials Reviews*. Taylor & Francis, 32(1), pp. 1–120. doi: 10.1179/095066087790150296.

Morales, R. D. *et al.* (1995) 'The slag foaming practice in EAF and its influence on the steelmaking shop productivity', *ISIJ international*. The Iron and Steel Institute of Japan, 35(9), pp. 1054–1062.

Morales, R. D. *et al.* (1997) 'A mathematical model for the reduction kinetics of iron oxide in electric furnace slags by graphite injection', *ISIJ international*. The Iron and Steel Institute of Japan, 37(11), pp. 1072–1080.

Morales, R. D. *et al.* (2002) 'Concept of dynamic foaming index and its application to control of slag foaming in electric arc furnace steelmaking', *Ironmaking & Steelmaking*. Taylor & Francis, 29(6), pp. 445–453. doi: 10.1179/030192302225004629.

Morales, R. D., Rodriguez-Hernández, H. and Conejo, A. N. (2001) 'A mathematical simulator for the EAF steelmaking process using direct reduced iron', *ISIJ international*. The Iron and Steel Institute of Japan, 41(5), pp. 426–436.

National Institute of standards and technology (2017) *Kinetics database:* Available at: http://kinetics.nist.gov/kinetics/index.jsp.

Pfeifer, H., Kirschen, M. and Simoes, J.-P. (2005) 'Thermodynamic analysis of electrical energy demand'.

Philbrook, W. O. and Kirkbride, L. D. (1956) 'Rate of FeO Reduction from a CaO-SiO2-Al2O3

Slag by Carbon-Saturated Iron', *JOM*, 8(3), pp. 351–356. doi: 10.1007/BF03377696.

Rao, Y. K. (1971) 'The kinetics of reduction of hematite by carbon', *Metallurgical Transactions*, 2(5), pp. 1439–1447. doi: 10.1007/BF02913373.

Richard Balzhiser, M. R. S. and J. E. (1972) *Chemical engineering thermodynamics: the study of energy, entropy, and equilibrium*. 1st edn. Prentice Hall.

Richard D. M. MacRosty, and C. L. E. S. (2005) 'Dynamic Modeling of an Industrial Electric Arc Furnace', *nd. Eng. Chem. Res.*, 44(21), pp. 8067–8083.

SAIL co. (2017) *Steel importance*. Available at: https://www.sail.co.in/learning-center/importance-steel.

Sain, D. R. and Belton, G. R. (1976) 'Interfacial reaction kinetics in the decarburization of liquid iron by carbon dioxide', *Metallurgical Transactions B*, 7(2), pp. 235–244. doi: 10.1007/BF02654922.

Sekino, K., Nagasaka, T. and Fruehan, R. J. (2000) 'Kinetics of the Reaction of C2H6, CH4-CO2 and CO-CO2-O2 Gases with Liquid Iron', *ISIJ International*, 40(4), pp. 315–321. doi: 10.2355/isijinternational.40.315.

SENER (2017) 'Balance nacional de energía 2016 (Versión preliminar)'. México, p. 136.

V. Sinelnikov, D. K. (2015) 'Modeling Viscosity of Converter Slag', *Archives of foundry engineering*, 15(4), pp. 119–124.

Smith, J. M., and H. C. V. N. (1996) *Introduction to chemical engineering thermodynamics*. 5th edn. McGraw Hill.

Steel University (2015) *Basic equipment and Operation*. Available at: https://steeluniversity.org/lessons/210-basic-equipment-and-operation-2/.

Tanaka, T. *et al.* (2016) 'Dynamic Changes in Interfacial Tension between Liquid Fe Alloy and

Molten Slag Induced by Chemical Reactions', *ISIJ International*. The Iron and Steel Institute of Japan, 56(6), pp. 944–952.

TENOVA (2017) *Consteel continous charging*. Available at: http://www.tenova.com/product/consteel-continuous-charging-system/.

Trejo, E. *et al.* (2012) 'A novel estimation of electrical and cooling losses in electric arc furnaces', *Energy*, 42(1), pp. 446–456. doi: http://dx.doi.org/10.1016/j.energy.2012.03.024.

Trejo, E. (2012) *Energy flows in steel industry: Mathemathical models and simulations in electric arc furnaces*. Instituto Tecnológico y de Estudios Superiores de Monterrey.

Vito Logar, D. D. and Skrjanc, I. (2012a) 'Development of an Electric Arc Furnace Simulator Considering Thermal, Chemical and Electrical Aspects', *ISIJ International*, 52(10), pp. 1924–1926. doi: 10.2355/isijinternational.52.1924.

Vito Logar, D. D. and Skrjanc, I. (2012b) 'Modeling and Validation of an Electric Arc Furnace: Part 1, Heat and Mass Transfer', *ISIJ International*, 52(3), pp. 402–412. doi: 10.2355/isijinternational.52.402.

Vito Logar, D. D. and Skrjanc, I. (2012c) 'Modeling and Validation of an Electric Arc Furnace: Part 2, Thermo-chemistry', *ISIJ International*, 52(3).

Westley, F. (1980) 'Table of recommended rate constants for chemical reactions ocurringin combustion'. National standard Reference Data System, p. 122.

White, W. B., Johnson, S. M. and Dantzig, G. B. (1958) 'Chemical Equilibrium in Complex Mixtures', *The Journal of Chemical Physics*. American Institute of Physics, 28(5), pp. 751–755. doi: 10.1063/1.1744264.

Wu, Y. K. and Lacroix, M. (1995) 'Numerical simulation of the melting of scrap metal in a circular furnace', *International Communications in Heat and Mass Transfer*, 22(4), pp. 517–525. doi: https://doi.org/10.1016/0735-1933(95)00037-Y.

Zhang, Y. and Fruehan, R. J. (1995) 'Effect of the bubble size and chemical reactions on slag foaming', *Metallurgical and Materials Transactions B*, 26(4), pp. 803–812. doi: 10.1007/BF02651727.